90% *SNR* Improvement with Multi-Port Hall Plates

Udo Ausserlechner

Sense and Control Department, Infineon Technologies AG, Villach, Austria
Email: udo.ausserlechner@infineon.com

Abstract

For Hall plates, the ratio of signal over thermal noise is determined by material properties, thickness, layout geometry, magnetic field, and the electric power at which the plate is operated. For traditional Hall plates with four contacts, the optimum choice is a symmetrical device with medium-sized contacts. This paper shows that the signal-to-noise-ratio (*SNR*) can be further increased by up to 90% for Hall plates with more than four contacts. Supply currents flow through several pairs of contacts, while a signal conditioning circuit taps output voltages at all pairs of contacts and sums them up. We compute the total thermal noise of the sum of correlated noise voltages and relate it to the total magnetic sensitivity. We also prove that for electrically linear devices a spinning current scheme cancels out zero point errors (offset errors) in a strict sense. All our investigations use the definite resistance matrix of multi-port Hall plates. We develop an analytical theory based on recent advances in the theory of Hall plates, and then we compute the integrals and matrices numerically for symmetrical Hall plates with six to 40 contacts. We also present measurements in accordance with our theory.

Keywords

Multi-Port Hall Plates, Noise Correlation, Noise Efficiency, Signal to Noise Ratio, Spinning Scheme, Thermal Noise, Toeplitz Matrix

1. Introduction

In this work we look for ways about how to get less noisy signals from Hall plates. On the one hand we want to maximize the output signal per milli-Tesla of impressed magnetic field; on the other hand we want to minimize the noise in the signal while keeping the power consumption of the Hall plate constant. The focus of this paper is an optimum topology of the Hall plate that can be used in

smart silicon Hall sensor circuits—we do not search for special material compositions, which provide large Hall mobility, such as III-V-heterojunctions, Graphene, or other 2-DEGs.

It is known that the main noise in macroscopic Hall plates with sizes in the order of millimeters is thermal noise [1]. In modern semiconductor technology Hall plates are commonly only 20 μm to 150 μm large and 1 μm thick with low n-doping of 5×10^{15} - 10^{17}/cm³. This can give a relatively low number of one million charge carriers in the active region of the device. Therefore we also note a strong 1/f-noise contribution, as with all other micro-electronic circuit devices. However, it is possible to operate a Hall plate at frequencies between 1 kHz and 1 MHz thereby cancelling out 1/f-noise. A simple way is to switch the Hall plate on and off at this frequency and process the output voltage with a sample and hold circuit or a simple low-pass filter. A more common method is the spinning current scheme, which greatly reduces the zero-point (offset) error of the Hall plate, and simultaneously it cancels out 1/f-noise, too [2] [3]. Note that all these operating modes allow for a detection of static and low frequency magnetic fields even though the Hall plate is electrically operated at elevated frequencies. Therefore we may ignore 1/f-noise of Hall plates and focus on thermal noise only.

An optimization of the signal-to-thermal-noise-ratio (*SNR*) is known for conventional Hall plates with four contacts [4]. For maximum *SNR* the Hall plate should be symmetric with medium-sized contacts. That means, it should have identical input and output resistance and the average potential of both output contacts should be half of the supply voltage; *i.e.* the common mode potential of the differential output signal should be exactly in the center between both supply potentials. The size of the contacts should be chosen such that the input and output resistances are $\sqrt{2}$ times as the sheet resistance $R_{\text{sheet}} = \rho/t_H$ (ρ is the specific resistivity of the material in the Hall plate at zero impressed magnetic field and t_H is the thickness of the Hall plate). There are many shapes, which fulfill these requirements. The most common ones are circles, crosses, octagons, and rectangles with specific sizes of contacts as shown in Figure 5 of [4]. Most of them have 90˚ symmetry. According to Wick, Hall plates whose shapes are linked via conformal transformations have identical impedances and magnetic field sensitivities [5]. Thus, they also have identical *SNR*s. Hence, we may focus on circular Hall plates with peripheral contacts. Once we find an optimum one, we may derive other equivalent shapes of Hall plates by conformal transformations. The optimum circular Hall plate with four contacts has contacts extending over 45˚ separated by insulating arcs of the same size (**Figure 1(a)**). These are surprisingly large contacts, which reduce the Hall signal per supply current by one third compared to the maximum possible one for point-sized contacts. On the other hand, point-sized contacts give infinitely large impedance, which leads to large thermal noise. The best trade-off between Hall signal and noise turns out to be medium-sized contacts that cover 50% of the perimeter of the disk.

For Hall plates with three contacts the Hall signal and the thermal noise were
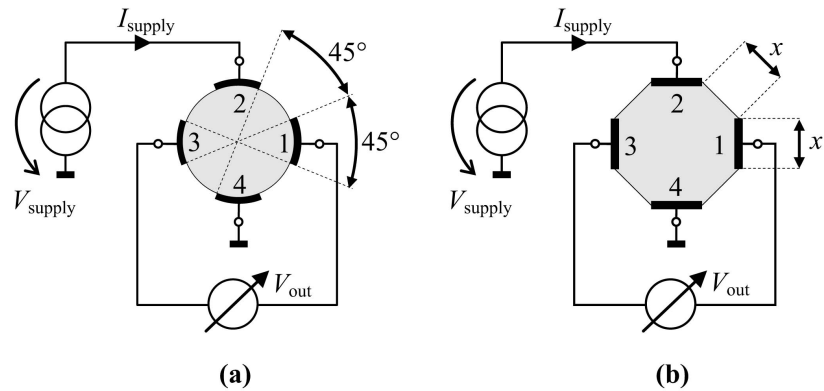
Figure 1. Conventional Hall plates with four contacts in conventional operating mode "single current input, single voltage output". At this particular size of contacts they have maximum *SNR* at weak magnetic field. The figure shows two out of infinitely many equivalent shapes which are obtainable by conformal transformation: circular and octagonal Hall-effect regions. Both times the contacts are equally large as the insulating arcs between them. Input and output resistances are equal to $\sqrt{2}R_{\text{sheet}}$ and the weak field Hall geometry factor is $G_{H0} = 2/3$ [4].

studied in [6] [7]. The maximum *SNR* per Watt of dissipated power is obtained for symmetric devices operated like in **Figure 2**, but this optimum is still 1.51 times lower than for optimized Hall plates with four contacts. This is interesting because contacts are usually believed to deteriorate the Hall signal. Nevertheless the comparison of Hall plates with three and four contacts shows that the device with more contacts has better *SNR*.

Hall plates with eight contacts are reported in [8] [9]. They are supposed to have exceptionally low offset errors close to 1 µT when operated in an 8-phase spinning scheme [8]. In each phase current flows through two opposite contacts while voltage is tapped at two opposite contacts perpendicular to a line through the current carrying contacts (**Figure 3**). The other four contacts are not used in this phase. In seven subsequent phases all contacts are moved by one instance clock-wise with regard to the preceding phase. Finally the output voltages of all eight phases are added, thereby very efficiently reducing offset errors.

Hall plates with more than eight contacts were used in spinning current schemes studied by Munter [10] [11]. But still he used only single pairs of output contacts in each phase (single input current, single output voltage).

Another idea uses an integer multiple of four contacts, e.g. 8, 12, 16 … contacts, whereby every fifth contact is connected to the same terminal (**Figure 4**). An example of eight contacts is shown in [12] (see also Figures 3-4b in [10]). In general, contacts 1, 5, 9, … are connected to a first terminal, contacts 2, 6, 10 ... are connected to a second terminal, contacts 3, 7, 11, ... to a third terminal, and contacts 4, 8, 12, … to a fourth terminal. Operation is analogous to a conventional Hall plate with four contacts: current is supplied through the even terminals and voltage is tapped across the odd terminals, and vice versa. We will show in **Appendix B** that regardless of the number of contacts this kind of device does not have better *SNR* than optimum Hall plates with four contacts.
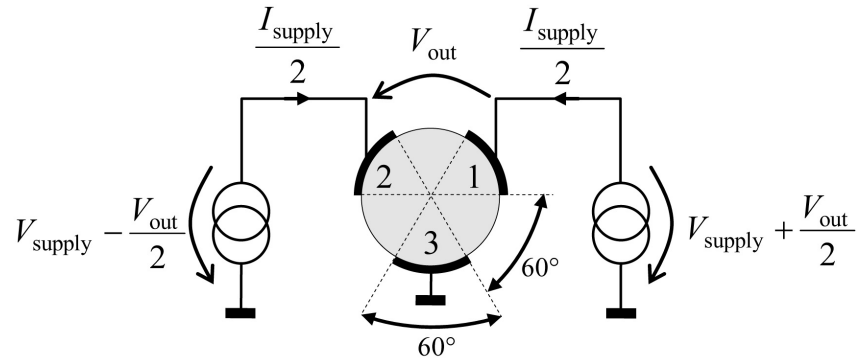
Figure 2. Circular Hall plate with three contacts, supplied by two equal currents, and with one output voltage (double current input, single voltage output). For maximum *SNR* at weak magnetic field the contacts are as large as the insulating arcs between them. The power dissipation is $P_{\text{supply}} = V_{\text{supply}} I_{\text{supply}}$. Thus the input resistance is $P_{\text{supply}} / I_{\text{supply}}^2 = \sqrt{3} R_{\text{sheet}} / 2$, the output resistance is $2 R_{\text{sheet}} / \sqrt{3}$, and the weak field Hall geometry factor is $G_{H0}^{(3C)} \cong 0.622157$ [6] [7].


(a)   **(b)**
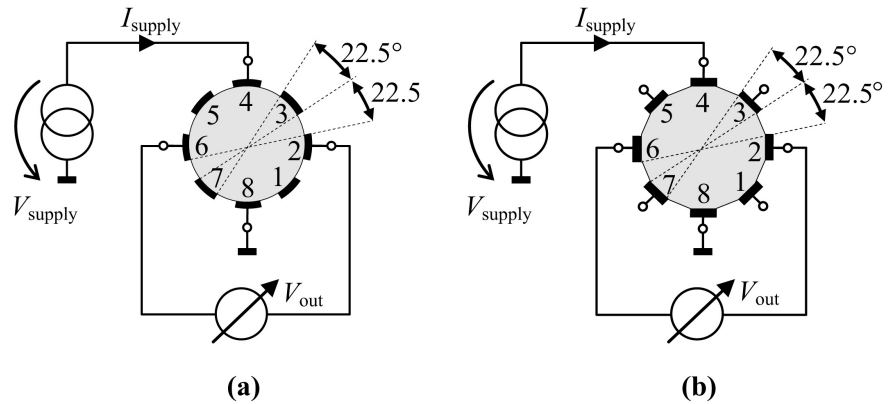
Figure 3. Symmetric Hall plates with eight contacts. The figure shows two out of infinitely many equivalent shapes, which are obtainable by conformal transformations: circular and polygonal Hall-effect regions. Both times the contacts are equally large as the insulating arcs between them. Input and output resistances are equal to $1.84776 \times R_{\text{sheet}}$ and the Hall geometry factor is $G_{H0} = 0.820246$ (both at weak magnetic field, see **Table 1** and **Table 2**).

Yet another idea uses Hall plates with a large numbers of contacts, where voltage is tapped only across a single pair of contacts while all other contacts carry supply current (**Figure 5**) [13] (multiple input currents, single output voltage). The goal of the authors was to avoid large current contacts because they reduce the Hall signal by their short-circuiting action. We will show in **Appendix C** that these topologies do not give better noise performance per Watt than optimized traditional Hall plates with four contacts from **Figure 1**.

Occasionally the question pops up if measuring current instead of voltage at the output contacts of a Hall plate might improve its performance [14]. As long as the Hall plate is a passive device with linear electric properties, its voltages and currents are linked via a linear resistance matrix. In contrast to the statements in
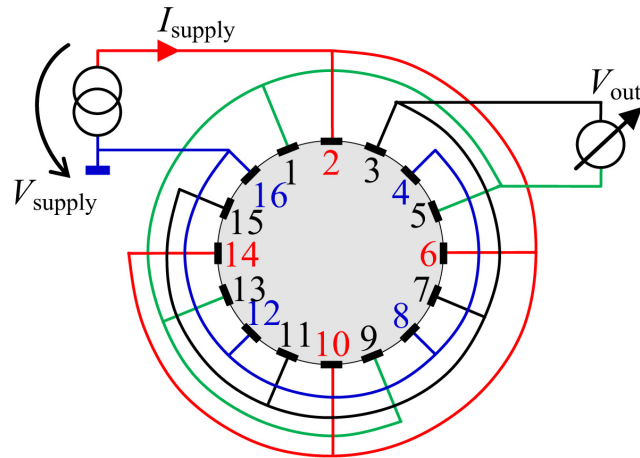
Figure 4. Hall plates with an integer multiple of four contacts where every 5th contact is connected to the same terminal. If contacts are equally large as insulating arcs the device has the same *SNR* as the Hall plates in **Figure 1** regardless if the plate has 8, 12, 16, ... $4n$ contacts. Input and output resistances are equal to $\sqrt{2}R_{sheet}/n$ and the Hall geometry factor equals $2/(3n)$ (all at weak magnetic field, see **Appendix B**). For large numbers of contacts the current tends to flow near the perimeter. Then we may cut out the center portion of the plate. Then, we may also place contacts on the inner boundary—this gives Hall voltages with inverted polarity.
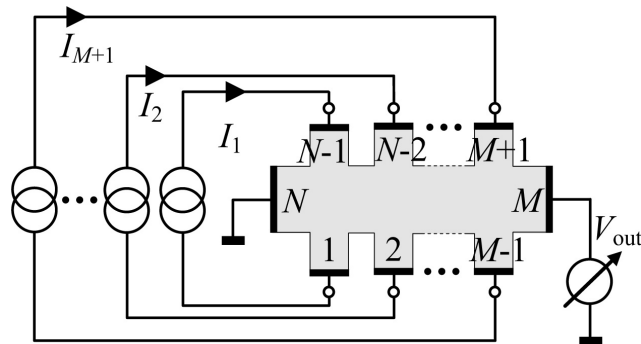

Figure 5. Hall-effect devices with many supply contacts and only a single pair of output contacts after [13]. This concept has no better *SNR* then classical Hall plates with four contacts (see **Appendix C**).

[14] current mode operation does *not* change the boundary conditions of the Hall effect region when compared to voltage mode operation: the electric field is still perpendicular to the contacts and the current streamlines are still tangential to the insulating boundary. The resulting electric potential and the current stream-lines are a mere superposition of currents and voltages applied to the contacts. Thus, according to the theory of linear electric networks, the *SNR* should be identical no matter if we measure the output current or voltage. We enlarge on this issue in **Appendix D**.

The initial idea of this work is to supply multi-port Hall plates with electric current through only two opposite contacts like in [8] [10]. However, in contrast to [8] [10] we use *all* other contacts as outputs, because they *all* provide Hall

signals *without additional power dissipation*. If we add all output signals we get more net signal per watt, and if the correlation between the noise voltages at all output ports is low this should improve the *SNR*. For our systematic theoretical study in Section 2 we apply an ingenious method of calculation which was invented only recently by Homentcovschi, Bercia & Murray [15] [16]. It is ideally suited for our purpose because it works for Hall plates with an arbitrary number of contacts. In Section 3 we compute the correlation of thermal noise between various ports of a multi-port Hall plate. In Section 4 we define what we mean by optimum *SNR* and compute it for the multi-port Hall plate. In Section 5 we derive a spinning scheme for multi-port Hall plates. Section 6 studies the general idea of multi-port Hall plates with multiple input currents and multiple output voltages, which gives even larger *SNR* than in preceding sections.. Section 7 gives an experimental verification of our theory. **Appendix A** computes the resistances of the equivalent network for multi-port Hall plates at zero magnetic field. It also shows the particular type of Toeplitz symmetry in their conductance matrix. **Appendices B-D** prove that various Hall plates discussed in the literature have less *SNR* than the multi-port Hall plates. **Appendix E** explains how to compute the optimum weighing coefficients in the linear combination of output voltages from multiple ports. **Appendix F** shows an algorithm to optimize currents and weighing coefficients from circuits of Section 6.

2. Hall Signals in a Multi-Port Hall Plate

We consider circular Hall plates with $N = 2M$ contacts, where N is an even number and M is greater than 1 (see **Figure 6**). All contacts are labelled in sequential order along the periphery. The N-th contact is grounded and supply current is injected into the M-th contact. We define $M - 1$ output ports of the Hall plate: The k-th output port comprises the k-th and the $(N\text{-}k)$-th contact. The potential at each contact is labelled V_k. Then the output voltage at the k-th port is $V_{\text{out},k} = V_k - V_{N-k}$. The overall output of the Hall plate is the linear combination of outputs of all ports $V_{\text{out}} = \sum_{k=1}^{M-1} c_k V_{\text{out},k}$. An electronic circuit can readily sum up all the contributions of all ports as sketched in **Figure 6**. Let us set $c_k = 1$ to start with.

For a conventional Hall plate with four contacts we have $N = 4$ and $M = 2$ and only one output port $V_{\text{out}} = V_{\text{out},1} = V_1 - V_3$. In this section we consider only symmetric devices where the voltages across the output ports vanish in the absence of impressed magnetic field. For conventional Hall plates with four contacts it holds

$$V_{\text{out}} = R_{\text{sheet}} G_H \tan(\theta_H) I_{\text{supply}} \tag{1}$$

with the Hall angle $\theta_H = \arctan(\mu_H B_\perp)$, the Hall mobility μ_H, and the magnetic flux density $B_\perp$ perpendicular to the Hall plate. The Hall geometry factor G_H is a number between 0 and 1 and it accounts for the loss in output voltage caused by the finite size of the contacts. Large supply contacts short the Hall electric field and large output contacts shunt a considerable portion of the supply
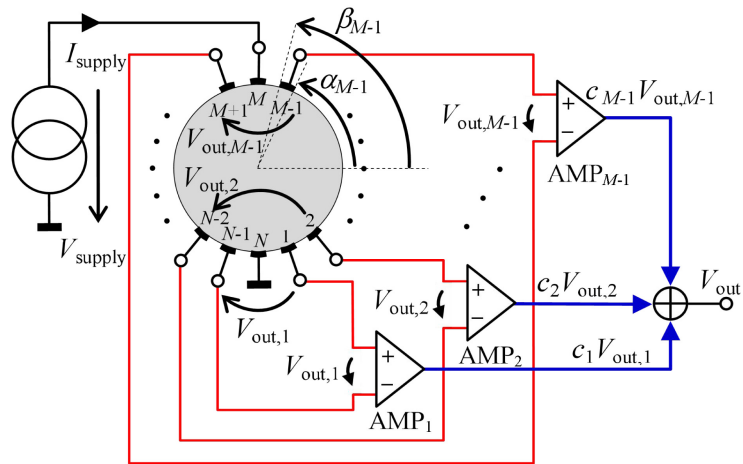
Figure 6. Regular circular Hall plate with $N = 2M$ contacts in operating mode "single input current, multiple output voltages". Current is supplied at contacts M and N. Voltages are tapped at all other contacts and summed up with a circuit of M-1 amplifiers (AMPs). The gains c_k of the AMPs are weighing coefficients in the linear combination of signals from all output ports. Angles a_k, β_k are given in (2).

current away from the Hall effect region, where it does not contribute to the Hall signal. If the contacts are point-sized and located on the boundary it holds $G_H = 1$ [17]. Also at very strong impressed magnetic field G_H tends to 1 [17]. In both cases the impedance of the Hall plate rises and this leads to excessive thermal noise. Therefore we have to use contacts which are neither too large nor too small—we have to trade off impedance and Hall signal. For circular Hall plates with four contacts it is known that optimum *SNR* at weak magnetic field is achieved for the device in **Figure 1** [4]. Its contacts are equally large as the insulating arcs between the contacts. Therefore we keep this high degree of symmetry also for the multi-port Hall plates. Then the vertices of the contacts are at angles (see **Figure 6**)

$$\alpha_k = 360° \times (k-1)/N \quad \text{and} \quad \beta_k = \alpha_k + 180°/N \; ; \; k = 1, 2, \cdots, N \; . \tag{2}$$

Analogous to (1) we define the Hall geometry factor for the k-th port.

$$V_{\text{out},k} = R_{\text{sheet}} G_{H,k} \tan(\theta_H) I_{\text{supply}} \tag{3}$$

Although all contacts are equally large, they do not have the same Hall signal. Ports closer to the supply contacts have less Hall signal than ports mid-way between both supply contacts, because in the proximity of the supply contacts their short-circuiting action reduces the Hall signal. We write the sum of voltages of all ports analogous to (1)

$$V_{\text{out}} = \sum_{k=1}^{M-1} V_{\text{out},k} = R_{\text{sheet}} (M-1) G_H \tan(\theta_H) I_{\text{supply}} \tag{4a}$$

$$G_H = \frac{1}{M-1} \sum_{k=1}^{M-1} G_{H,k} \tag{4b}$$

In (4b) we normalize the total Hall geometry factor by the number of output

ports in order to keep it less or equal to 1. In the sequel we refer to it as the average Hall geometry factor of the multi-port Hall plate in operating mode "single input current, $M-1$ output voltages". For Hall plates with four contacts (4a, b) become identical to (1).

We may compute the potentials at all contacts in response to the supply current by use of the definite resistance matrix R of rank $N-1$.

$$V = \begin{pmatrix} V_1 \\ V_2 \\ \vdots \\ V_{N-1} \end{pmatrix} = \begin{pmatrix} R_{1,1} & R_{1,2} & \cdots & R_{1,N-1} \\ R_{2,1} & R_{2,2} & \cdots & R_{2,N-1} \\ \vdots & \vdots & \ddots & \vdots \\ R_{N-1,1} & R_{N-1,2} & \cdots & R_{N-1,N-1} \end{pmatrix} \cdot \begin{pmatrix} I_1 \\ I_2 \\ \vdots \\ I_{N-1} \end{pmatrix} = R \cdot I \tag{5}$$

In the operating mode of **Figure 6** all elements of the current vector I vanish except $I_M = I_{\text{supply}}$. With (3) the Hall geometry factor of each port follows from the resistance matrix.

$$G_{H,k} = \frac{R_{k,M} - R_{N-k,M}}{R_{\text{sheet}} \tan(\theta_H)} \tag{6}$$

The resistance matrix of a circular Hall plate with N contacts from **Figure 6** can be computed in an elegant way with [16]

$$R = \frac{R_{\text{sheet}}}{\cos(\theta_H)} B^{-1} C \tag{7}$$

with the elements of the matrices B and C given by

$$B_{k,m} = \int_{\alpha_m}^{\beta_m} \frac{h(\tau)\,d\tau}{\sin((\tau - \beta_N)/2)\sin((\tau - \beta_k)/2)} \tag{8}$$

$$C_{k,m} = -\sum_{q=m}^{N-1} \int_{\beta_q}^{\alpha_{q+1}} \frac{h(\tau)\,d\tau}{\sin((\tau - \beta_N)/2)\sin((\tau - \beta_k)/2)} \tag{9}$$

$$h(\tau) = \prod_{j=1}^{N} \left| \frac{\sin((\tau - \beta_j)/2)}{\sin((\tau - \alpha_j)/2)} \right|^{\frac{1}{2} + \frac{\theta_H}{\pi}} \tag{10}$$

for $k, m = 1, \cdots, N-1$. We use a different sign of θ_H than [16], because the charge carriers in n-doped silicon are negative. We cannot solve the integrals in closed form, but the numerical evaluation for small and moderate Hall angles is simple with program codes like MATHEMATICA. The results for Hall geometry factors of all ports for Hall plates with up to $N = 40$ contacts are given in **Table 1** and **Figure 7**. Thereby, we used a small Hall angle of 0.09°, which corresponds to weak magnetic field where noise and *SNR* are most relevant in practice. We denote the weak field conditions by a subscript "0".

$$\lim_{B_\perp \to 0} G_H = G_{H0} \quad \text{and} \quad \lim_{B_\perp \to 0} G_{H,k} = G_{H0,k} \tag{11}$$

In **Figure 7** we plotted $G_{H0,k}$ versus the common mode *cm*, which we define as

Table 1. Weak field Hall geometry factors $G_{H0,k}$ of all ports for symmetric Hall plates of **Figure 6** (computed with (6)-(10) at 0.09° Hall angle). The operating mode is "single input current, $M - 1$ output voltages". Each line corresponds to a Hall plate with $N = 2M$ contacts. Hall geometry factors of ports with larger index are labelled as non applicable "n.a". *Example*: A Hall plate with $N = 12$ contacts has 5 output ports. Due to symmetry it holds $G_{H0,5} = G_{H0,1}$, and $G_{H0,4} = G_{H0,2}$. Hence, only $G_{H0,1}$, $G_{H0,2}$, and $G_{H0,3}$ are given explicitly.

| N	$G_{H0,1}$	$G_{H0,2}$	$G_{H0,3}$	$G_{H0,4}$	$G_{H0,5}$	$G_{H0,6}$	$G_{H0,7}$	$G_{H0,8}$	$G_{H0,9}$	$G_{H0,10}$
4	0.666667	n.a.	n.a.	n.a.	n.a.	n.a.	n.a.	n.a.	n.a.	n.a.
6	0.736477	$G_{H0,1}$	n.a.	n.a.	n.a.	n.a.	n.a.	n.a.	n.a.	n.a.
8	0.757940	0.820246	$G_{H0,1}$	n.a.	n.a.	n.a.	n.a.	n.a.	n.a.	n.a.
10	0.767379	0.847737	$G_{H0,2}$	$G_{H0,1}$	n.a.	n.a.	n.a.	n.a.	n.a.	n.a.
12	0.772378	0.860488	0.878089	$G_{H0,2}$	$G_{H0,1}$	n.a.	n.a.	n.a.	n.a.	n.a.
14	0.775349	0.867537	0.892522	$G_{H0,3}$	$G_{H0,2}$	$G_{H0,1}$	n.a.	n.a.	n.a.	n.a.
16	0.777259	0.871875	0.900677	0.907982	$G_{H0,3}$	$G_{H0,2}$	$G_{H0,1}$	n.a.	n.a.	n.a.
18	0.778561	0.874748	0.905792	0.916832	$G_{H0,4}$	$G_{H0,3}$	$G_{H0,2}$	$G_{H0,1}$	n.a.	n.a.
20	0.779489	0.876753	0.909237	0.922450	0.926163	$G_{H0,4}$	$G_{H0,3}$	$G_{H0,2}$	$G_{H0,1}$	n.a.
22	0.780173	0.878211	0.911677	0.926273	0.932133	$G_{H0,5}$	$G_{H0,4}$	$G_{H0,3}$	$G_{H0,2}$	$G_{H0,1}$
24	0.780692	0.879306	0.913475	0.929008	0.936227	0.938366	$G_{H0,5}$	$G_{H0,4}$	$G_{H0,3}$	$G_{H0,2}$
26	0.781095	0.880149	0.914840	0.931041	0.939175	0.942663	$G_{H0,6}$	$G_{H0,5}$	$G_{H0,4}$	$G_{H0,3}$
28	0.781415	0.880813	0.915903	0.932598	0.941381	0.945773	0.947118	$G_{H0,6}$	$G_{H0,5}$	$G_{H0,4}$
30	0.781672	0.881346	0.916748	0.933818	0.943079	0.948111	0.950356	$G_{H0,7}$	$G_{H0,6}$	$G_{H0,5}$
32	0.781883	0.881779	0.917430	0.934795	0.944418	0.949919	0.952798	0.953697	$G_{H0,7}$	$G_{H0,6}$
34	0.782057	0.882137	0.917991	0.935589	0.945495	0.951351	0.954694	0.956225	$G_{H0,8}$	$G_{H0,7}$
36	0.782203	0.882436	0.918456	0.936245	0.946375	0.952507	0.956201	0.958193	0.958823	$G_{H0,8}$
38	0.782327	0.882688	0.918848	0.936792	0.947105	0.953455	0.957420	0.959760	0.960851	$G_{H0,9}$
40	0.782432	0.882903	0.919180	0.937255	0.947717	0.954244	0.958424	0.961033	0.962470	0.962929
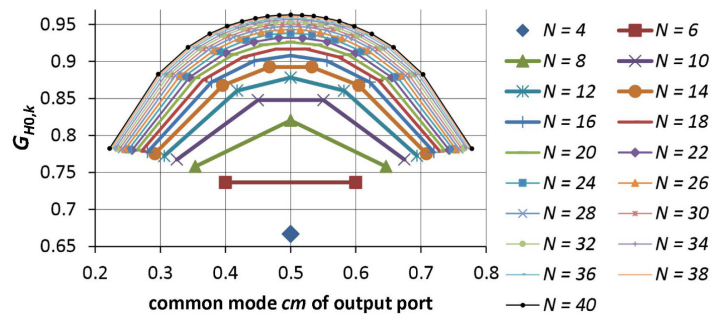
Figure 7. Weak field Hall geometry factors $G_{H0,k}$ of all output ports plotted versus common mode cm of the output ports. The Hall plates and their operating mode "single input current, multiple output voltages" are shown in **Figure 6**. The numbers of contacts are $N = 4, 6, 8, ..., 40$. Numerical values in **Table 1**. $G_{H0,k}$ is defined in (6) and (11), cm is defined in (12).

$$cm = \frac{(V_k + V_{N-k})/2 - V_N}{V_M - V_N} \tag{12}$$

Thus, the common mode is the ratio of average potential of a port over the supply voltage drop. It is a value between 0 and 1. Obviously, the Hall signal drops for contacts closer to the current supply contacts. For $N > 4$ we have more output ports and larger Hall signal per output port. The average weak field Hall geometry factor versus N is shown in **Figure 8**. It starts at 2/3 for a Hall plate with four contacts and increases beyond 0.9 for $N = 40$. It is likely but not yet proven that it goes to 1 for $N \to \infty$. The same **Figure 8** also plots the input resistance R_{in} of the Hall plate with N contacts in units of the sheet resistance.

$$R_{in} = \frac{V_M - V_N}{I_M} = R_{M,M} \tag{13}$$

Although the sizes of the contacts shrink with N also their spacings shrink. Thus, the impedance between the supply contacts goes up only moderately with N (see the logarithmic fit formula in **Figure 8**).

3. The Thermal Noise of a Multi-Port Hall Plate

At weak magnetic field the Hall plate is a resistive domain with N contacts. Then its deterministic electrical behavior is fully described by its resistance matrix. It links the voltages at the contacts with the currents into the contacts in a linear fashion. This corresponds to a resistor network with resistances $r_{i,j}$ between pairs (i, j) of contacts. Thus, a Hall plate with N contacts corresponds to a resistor network with $(N-1) + (N-2) + \cdots + 2 + 1 = N * (N-1)/2$ resistors. The symmetry of the Hall plate is reflected by the symmetry of the resistor network. For the Hall plates of **Figure 6** the resistor network has only $\lfloor N/2 \rfloor$ different resistance values (where $\lfloor x \rfloor$ means the integer part of x). For $N = 3$ to 21 they are given in **Appendix A**. There we also explain how to compute the resistance values of the network from the definite resistance matrix R.

In his seminal paper, Nyquist showed with general laws of thermodynamics that in thermal equilibrium each resistor $r_{i,j}$ between contacts i and j acts as a
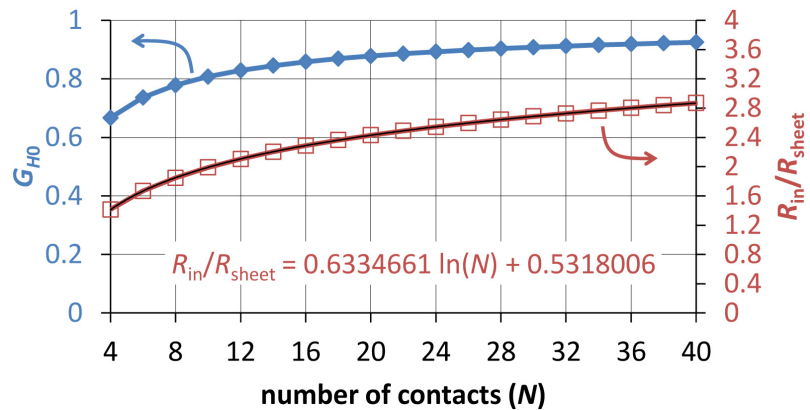

Figure 8. Average weak field Hall geometry factor G_{H0} of the Hall plates from **Figure 6**. Also: normalized input resistance of these Hall plates at weak magnetic field. Both are plotted versus the number of contacts. Numerical values in **Table 2**. G_{H0} is computed with (4b), (6), and (7)-(10). R_{in} is computed with (13) and (7)-(10).

thermal noise source with a built-in noise voltage $n(t)$ versus time t [18]. Its mean value vanishes

$$\overline{n_{i,j}} = \lim_{t\to\infty} \frac{1}{t} \int_{\tau=0}^{t} n_{i,j}(\tau)\,\mathrm{d}\tau = 0 \tag{14a}$$

Thermal noise is characterized by its noise power, which is the mean of its squared value

$$\overline{n_{i,j}^2} = \lim_{t\to\infty} \frac{1}{t} \int_{\tau=0}^{t} n_{i,j}^2(\tau)\,\mathrm{d}\tau = 4k_b T r_{i,j} \Delta \tag{14b}$$

where k_b is Boltzmann's constant, T is the absolute temperature, and Δ is the observation bandwidth. The noise voltage is the square-root of (14b) which is also called the noise rms voltage (root mean squared). The noise voltages of different resistors in a network are uncorrelated, which means that their noise powers simply add up,

$$\overline{\left(n_{i,j} + n_{k,\ell}\right)^2} = \overline{n_{i,j}^2} + \overline{n_{k,\ell}^2} = 4k_b T \left(r_{i,j} + r_{k,\ell}\right)\Delta \tag{15a}$$

because they are uncorrelated

$$\overline{n_{i,j} n_{k,\ell}} = \lim_{t\to\infty} \frac{1}{t} \int_{\tau=0}^{t} n_{i,j}(\tau) n_{k,\ell}(\tau)\,\mathrm{d}\tau = 0 \tag{15b}$$

Johnson said that whenever we look through a port into a complex network the thermal noise voltage at this port is the same as if we replace the network by the real part of its impedance at this port [19]. Thus the noise voltage at the k-th output port of our Hall plate at zero magnetic field is given by (14b) if we replace $r_{i,j}$ by the output resistance $R_{\text{out},k}$ of this port.

However, a single resistor of the network will contribute to the noise on all ports. Therefore the noise voltages at the ports will exhibit some correlation. If we label the noise voltages at ports k and ℓ by n_k and n_ℓ, respectively, it holds for the noise power of the sum of both ports

$$\overline{\left(n_k + n_\ell\right)^2} = \overline{n_k^2} + 2\overline{n_k n_\ell} + \overline{n_\ell^2} \neq \overline{n_k^2} + \overline{n_\ell^2} = 4k_b T \left(R_{\text{out},k} + R_{\text{out},\ell}\right)\Delta \tag{16}$$

Hence, we would make an error in the noise calculation if we accounted only for the output resistances of the ports. A correct calculation would have to compute the noise in the sum of port voltages caused by each of the $N*(N-1)/2$ resistors separately, and add up the squares of these noise contributions. To this end one has to compute the resistances of the network and the transfer functions of their noise voltages to all output ports—which is some computational effort without physical insight. We did it as a check for the results of the following paragraphs but it is not worthwhile to report it in detail.

A more rewarding method to compute the noise in the sum of all output ports is shown in **Figure 9**. There we add up the voltages of all ports by ideal transformers. Ideal transformers are loss-less and noise-less. Thus, they do not alter the power of the thermal noise in the output signal. The big advantage of ideal transformers is that we can connect their outputs in series thereby adding up all
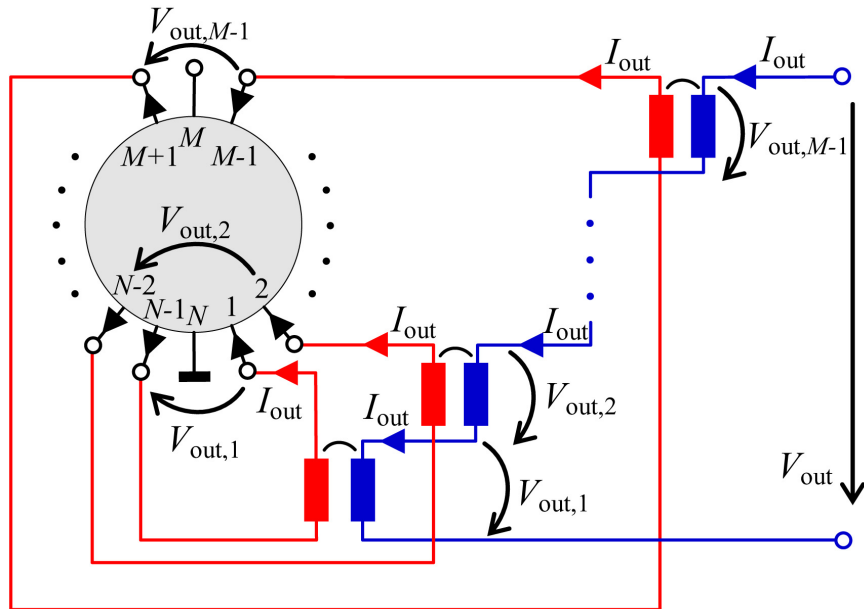
Figure 9. A network of ideal transformers adds up the voltages of all output ports of a Hall plate from **Figure 6**. Its output resistance determines the thermal noise of the sum of all output ports.

port voltages with galvanic isolation. Note that the circuit in **Figure 9** is not supposed to be implemented in practice. It is just a theoretical tool to compute with least effort the thermal noise in the sum of voltages of all output ports. Next, we can apply the finding of Johnson: the noise is equivalent to the output resistance. We do not need the resistor circuit for the output resistance. It is simpler to use the definite resistance matrix $\boldsymbol{R}$. With **Figure 9** we write

$$
\boldsymbol{V} = \begin{pmatrix} R_{1,1} & \cdots & R_{1,N-1} \\ \vdots & \ddots & \vdots \\ R_{M-1,1} & \cdots & R_{M-1,N-1} \\ R_{M,1} & \cdots & R_{M,N-1} \\ R_{M+1,1} & \cdots & R_{M+1,N-1} \\ \vdots & \ddots & \vdots \\ R_{N-1,1} & \cdots & R_{N-1,N-1} \end{pmatrix} \cdot \begin{pmatrix} I_{\text{out}} \\ \vdots \\ I_{\text{out}} \\ 0 \\ -I_{\text{out}} \\ \vdots \\ -I_{\text{out}} \end{pmatrix} \tag{17}
$$

During the measurement of the output resistance the transformers force the current I_{out} into all contacts $1, 2, \cdots, M-1$ and out of all contacts $M+1, M+2, \cdots, N-1$. No current flows into contacts M and N. We sum up all port voltages to get the total output voltage V_{out}. This is the voltage, which an Ohm-meter would see during a measurement of R_{out}, while it forces current I_{out} into the output terminals of the circuit in **Figure 9**.

$$
R_{\text{out}} = \frac{V_{\text{out}}}{I_{\text{out}}} = \sum_{j=1}^{M-1}\sum_{k=1}^{M-1} R_{j,k} + \sum_{j=M+1}^{N-1}\sum_{k=M+1}^{N-1} R_{j,k} - \sum_{j=1}^{M-1}\sum_{k=M+1}^{N-1} R_{j,k} - \sum_{j=M+1}^{N-1}\sum_{k=1}^{M-1} R_{j,k} \tag{18}
$$

The thermal noise n_{out} in the sum of voltages of all output ports is then again given by (14b) if we replace $r_{i,j}$ by R_{out} of (18). The following scheme gives a bet-

ter impression on which elements of the definite resistance matrix are added and subtracted in (18).

$$
\begin{pmatrix}
R_{1,1} & \cdots & R_{1,M-1} & 0 & -R_{1,M+1} & \cdots & -R_{1,N-1} \\
\vdots & \ddots & \vdots & \vdots & \vdots & \ddots & \vdots \\
R_{M-1,1} & \cdots & R_{M-1,M-1} & 0 & -R_{M-1,M+1} & \cdots & -R_{M-1,N-1} \\
0 & \cdots & 0 & 0 & 0 & \cdots & 0 \\
-R_{M+1,1} & \cdots & -R_{M+1,M-1} & 0 & R_{M+1,M+1} & \cdots & R_{M+1,N-1} \\
\vdots & \ddots & \vdots & \vdots & \vdots & \ddots & \vdots \\
-R_{N-1,1} & \cdots & -R_{N-1,M-1} & 0 & R_{N-1,M+1} & \cdots & R_{N-1,N-1}
\end{pmatrix}
\tag{19}
$$

We can decompose the definite resistance matrix $\boldsymbol{R}$ into the sum of a matrix $\boldsymbol{R}_{\text{even}}$ with even symmetry and a matrix $\boldsymbol{R}_{\text{odd}}$ with odd symmetry.

$$
\boldsymbol{R} = \boldsymbol{R}_{\text{even}} + \boldsymbol{R}_{\text{odd}}
\tag{20a}
$$

$$
\left(\boldsymbol{R}_{\text{even}} \right)_{k,m} = \frac{R_{k,m} + R_{m,k}}{2} = \left(\boldsymbol{R}_{\text{even}} \right)_{m,k}
\tag{20b}
$$

$$
\left(\boldsymbol{R}_{\text{odd}} \right)_{k,m} = \frac{R_{k,m} - R_{m,k}}{2} = -\left(\boldsymbol{R}_{\text{odd}} \right)_{m,k}
\tag{20c}
$$

where all resistance elements are evaluated at the same magnetic field polarity $B_\perp$. The principle of reverse magnetic field reciprocity states [20]

$$
R_{k,m}\left(-B_\perp \right) = R_{m,k}\left(B_\perp \right)
\tag{21}
$$

Inserting (21) in (20b, c) gives

$$
\left(\boldsymbol{R}_{\text{even}} \right)_{k,m} = \frac{R_{k,m}\left(B_\perp \right) + R_{k,m}\left(-B_\perp \right)}{2}
\tag{22a}
$$

$$
\left(\boldsymbol{R}_{\text{odd}} \right)_{k,m} = \frac{R_{k,m}\left(B_\perp \right) - R_{k,m}\left(-B_\perp \right)}{2}
\tag{22b}
$$

At arbitrary magnetic field the even matrix $\boldsymbol{R}_{\text{even}}$ has only terms $B_\perp^{2p}$ and the odd matrix $\boldsymbol{R}_{\text{odd}}$ has only terms $B_\perp^{2p-1}$ with p being a non-negative integer. $\boldsymbol{R}_{\text{even}}$ reflects a reciprocal network, which consists only of resistors. However, at large magnetic field these resistors depend on the magnetic field—they exhibit magneto-resistance. Conversely, $\boldsymbol{R}_{\text{odd}}$ reflects an anti-reciprocal network, which can be modeled by gyrators or controlled sources [21]. $\boldsymbol{R}_{\text{odd}}$ describes the Hall effect in the Hall plate. Interestingly, the summing scheme in (19) cancels out all contributions of $\boldsymbol{R}_{\text{odd}}$ due to the odd symmetry (22b). Therefore the thermal noise of a Hall plate is independent of the Hall-effect. It only depends on the magneto-resistance effect. For the calculation of the noise voltage of Hall plates we only need the resistor network, not the gyrator network.

4. The Optimum Signal-to-Noise-Ratio of Multi-Port Hall Plates with Single Input Current

First, we define what we mean by optimum *SNR* since the answer depends on some boundary conditions. The Hall signal increases with the electric power at which one operates the Hall plate, whereas the thermal noise does not depend on

power. Thus, *SNR* rises with power. Large power leads to considerable self-heating and finally to the destruction of the Hall plate. We can push this limit further by more efficient means of cooling. Simple scaling of the size of the Hall plate reduces the power density and improves the heat delivery. In general, all these issues are irrelevant in industrial practice, because there, power and size relate to costs, which have to be kept small. For a Hall sensor circuit both supply voltage and supply current are already specified at the start of the design process. Therefore, we want to maximize *SNR* for a fixed value of input resistance of the Hall plate. With (4a), (14b), and (18) we write for multi-port Hall plates in **Figure 6**

$$SNR = \lim_{B_\perp \to 0} \frac{V_{out}}{n_{out}} = \mu_H B_\perp \sqrt{\frac{P_{Hall}}{4k_b T \Delta}} \eta_{1,M-1} \tag{23a}$$

$$\eta_{1,M-1} = \frac{(M-1)G_{H0}}{\sqrt{R_{out}/R_{sheet}} \sqrt{R_{in}/R_{sheet}}} \tag{23b}$$

We call $\eta_{1,M-1}$ the noise efficiency of the Hall plate with single input current and $M-1$ output voltages. It is independent of material properties and thickness of the Hall plate. In the weak field approximation it is also does not depend on the magnetic field. It is a mere function of the lateral geometry, *i.e.* the layout of the Hall plate, and of the operating mode, *i.e.* the number of supply currents and output voltages. In (23a) the Hall mobility is the only material parameter, and P_{Hall} is the power dissipated in the Hall plate.

Inserting (4b), (7) and (18) into (23a, b) gives the plot of *SNR* versus *N* in **Figure 10**. Even though the output resistance rises strongly with the number of contacts (parabolically) its noise is low enough for the *SNR* to increase versus *N*, too. For a large number of contacts this increase tends to 50%. In practice it might
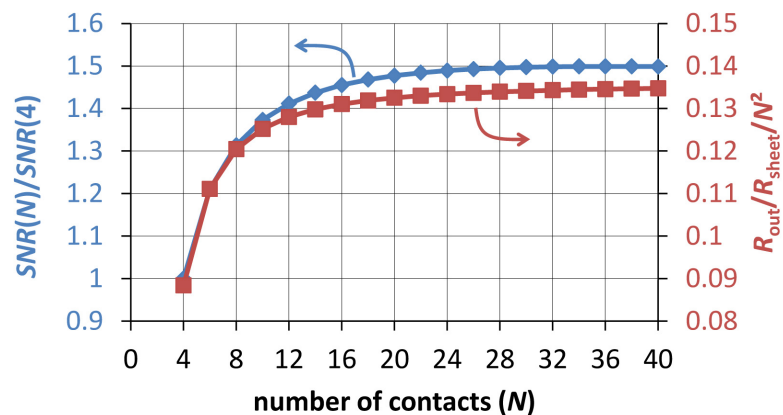
Figure 10. The *SNR* and the output resistance of Hall plates from **Figure 6**. The plot shows the ratio of *SNR* for Hall plates with *N* contacts over *SNR* for a Hall plate with four contacts. It also shows the ratio of output resistance over the product of sheet resistance and the square of the number of contacts. The operating mode is "single input current, *M*-1 output voltages". Numerical values in **Table 2**. Not visible in this scale: *SNR*(*N*) has a flat maximum in *N* = 36. The *SNR* is computed with (23b) and the output resistance is computed with (18).

Table 2. Electrical parameters for Hall plates of **Figure 6** (computed at 0.09° Hall angle): number of contacts $N = 2M$, average weak field Hall geometry factor G_{H0}, input and output resistances (for 1 Ω sheet resistance), noise efficiency $\eta_{1,M-1}$, and ratio of $SNR(N)$ with N contacts over $SNR(4)$ of conventional Hall plates with only four contacts—all for operating mode "single input current, $M-1$ output voltages". The last line gives the $SNR_{M/2}$ of Hall plates of **Figure 6**, if only the signal of the output port at 50% common mode is used for the output signal (this is port number $M/2$). $SNR(N)$ does *not* increase monotonically versus N. It has a flat maximum in $N = 36$. For $N = 4$ the noise efficiency $\eta_{1,M-1}$ is $\sqrt{2}/3 \cong 0.471$ [4].

N	4	6	8	10	12	14	16	20	36	40
G_{H0}	0.666667	0.736477	0.778709	0.807558	0.828764	0.845136	0.858229	0.878002	0.919062	0.924960
R_{in}	1.414215	1.666668	1.847760	1.988856	2.104399	2.202216	2.287017	2.428831	2.802727	2.869776
R_{out}	1.414215	4.000003	7.708066	12.52199	18.43434	25.44113	33.53998	53.00815	174.3981	215.6139
$\eta_{1,M-1}$	0.471404	0.570472	0.619014	0.647285	0.665309	0.677454	0.685939	0.696415	0.706696	0.706503
$\dfrac{SNR(N)}{SNR(4)}$	1.000000	1.210155	1.313128	1.373100	1.411334	1.437097	1.455096	1.477320	1.499129	1.498721
$\dfrac{SNR_{M/2}(N)}{SNR(4)}$	1.000000	n.a.	0.941683	n.a.	0.885150	n.a.	0.842198	0.808903	0.716911	0.711792

not be economical to use large $N > 20$ due to complexity and costs of the circuit. Yet, even small $N = 6, 8, 10$ has a notable improvement in SNR (21% to 37%) compared to the classical Hall plates with only four contacts. **Table 2** gives the numerical data for SNR, average weak field Hall geometry factor, and input and output resistances. Interestingly, the SNR has a flat maximum at $N = 36$. For more contacts it decreases, but this decrease is too small to be visibly in **Figure 10**. The last line in **Table 2** gives the SNR for the same Hall plates of **Figure 6** if only the single output port at 50% common mode provides the output signal (this is port number $M/2$). This is the case, which was studied in [10]. Then the SNR decreases monotonously with growing number of contacts, because the contacts become too small. For eight contacts (as in [8]) the loss in SNR is only 5.8% compared to optimum conventional Hall plates with four contacts.

In **Appendix E** we show that the SNR can be increased a bit further by multiplying the signals of the output ports with optimized weighing factors $c_k \neq 1$ prior to summing them up.

5. A Spinning Scheme for Offset Cancellation of Multi-Port Hall Plates with Single Input Current

Very low zero point error (offset error) is probably the strongest argument in favor of Hall plates when compared to magneto-resistive sensors. Due to small asymmetries of the Hall plate it has a relatively large *initial* offset in the order of several milli-Tesla. Yet, with the principle of spinning current Hall probes the *residual* offset can be reduced down to a few micro-Tesla [3] [8] [10]. The attractiveness of spinning schemes is very high for industrial manufacturing, because they implicitly reduce the offset error without need to measure it. During production a measurement of fields in the micro-Tesla range would be very costly, because standard equipment generates too strong magnetic disturbances.

Therefore it is of paramount importance to find spinning schemes for every new type of Hall-effect device. Luckily, we found the following one for multi-port Hall plates.

Let us define M operating phases of the spinning scheme, which are executed sequentially and their outputs $V_{\text{out,phase}(k)}$ are summed up. In the k-th operating phase current enters the Hall plate through contact k and leaves it through contact $k + M$, while all potentials at contacts $k + 1$ to $k + M - 1$ are added and all potentials at contacts $k + M + 1$ to $k + 2M - 1$ are subtracted. With (5) it holds

$$V_{\text{out,phase}(k)} = I_{\text{supply}} \sum_{j=k+1}^{k+M-1} R_{j,k} - R_{j,k+M} - R_{j+M,k} + R_{j+M,k+M} \qquad (24)$$

$$V_{\text{out,spin}} = \sum_{k=1}^{M} V_{\text{out,phase}(k)} \qquad (25)$$

In (25) no matrix element appears more than once, however, the indices go up to $3M - 1 > N$. We have to delete all elements where the first index equals N, because $V_N = 0$. We also have to delete all elements where the second index equals N, because the definite resistance matrix $\boldsymbol{R}$ already implicitly accounts for I_N as being the negative sum of all other currents. Moreover, we subtract N from any index which is greater than N. This takes account for the fact that some output contacts go into "a second loop" beyond the N-th contact, where of course contact $N + k$ is contact k. The resulting pattern of indices in (25) is shown for the case of $N = 12$ contacts in **Figure 11(a)**, **Figure 11(b)**. The first index in (24) corresponds to the horizontal axis and the second index to the vertical axis in **Figure 11(a)**, **Figure 11(b)**. A red "o" means that the matrix element is added and a blue "x" means that it is subtracted in (24). **Figure 11(a)** shows all matrix elements prior to subtracting N for indices greater than N. **Figure 11(b)**
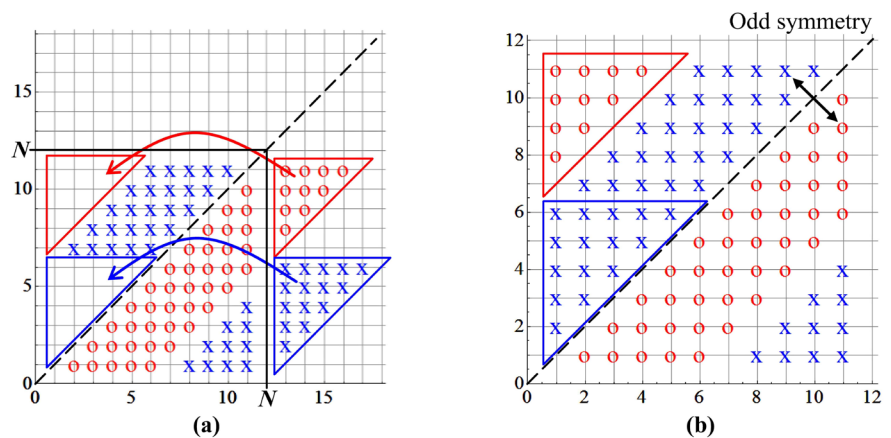
Figure 11. Occurence of matrix elements $R_{i,j}$ in the Hall spinning scheme (25) for M-1 output ports and $N = 12$. The horizontal axis in the plots gives the first index of $R_{i,j}$, the vertical axis gives the second index. The red "o" means that $R_{i,j}$ is added in (25), the blue "x" means that $R_{i,j}$ is subtracted. No element appears twice or more often. (a) Pattern of $R_{i,j}$ occurence prior to flipping elements with indices greater than N back into the "primitive" interval $[1, N - 1]$. (b) Final pattern of $R_{i,j}$ occurence after all elements are flipped into the interval $[1, N - 1]$. It shows the odd symmetry (26).

shows the final result when all indices are flipped back to the "primitive" interval $[1, N-1]$. There we note the symmetry: for every element $R_{i,j}$ there is a corresponding element $(-1) \times R_{j,i}$. Applying the principle of reverse magnetic field reciprocity (RMFR) [20] to these pairs gives

$$R_{i,j}\left(B_{\perp}\right) - R_{j,i}\left(B_{\perp}\right) = R_{i,j}\left(B_{\perp}\right) - R_{i,j}\left(-B_{\perp}\right) \tag{26}$$

In other words, the output signal of the spinning scheme $V_{\text{out,spin}}$ is an odd function of the magnetic field. Thus it vanishes at zero magnetic field. Therefore the zero point error (offset error) vanishes. This holds also for asymmetric Hall plates, because we did not make use of any symmetry of $\boldsymbol{R}$ other than the RMFR.

In (25) the sum goes only up to M, not up to $N = 2M$. This means that for each phase in (25) there is another one with inverted current flow polarity. In practice one will extend the sum over all N phases because it cancels out further errors caused by thermo-voltages, which were not accounted for in our simple linear theory.

6. Multi-Port Hall Plates with Multiple Input Currents and Multiple Output Voltages

In a very general general case, a circular Hall plate may have $N = 2M$ peripheral contacts. The N-th contact is grounded (see Figure 12). All other contacts are connected to current sources which determine the currents I_k ($k = 1, 2, \cdots, N-1$). M pairs of contacts are defined. A pair comprises contacts k and $N + 1 - k$ for $k = 1, 2, \cdots, M-1$. Voltmeters are connected to all contact pairs. Their voltage readings are multiplied by weighing factors c_k. These terms are summed up for all contact pairs to give the signal in a first operating phase. In total there are M operating phases, whereby the current sources and the voltmeters stay in place while the circular Hall plate rotates by one contact for each new operating phase. The overall output of this spinning scheme is the sum over all signals in all M operating phases.

We have many parameters that can be optimized. How can we determine the currents and weighing coefficients to achieve 1) zero offset error, and 2) maximum SNR? Obviously the currents are unique only up to a common multiplicative factor, which would neither change offset nor SNR. Therefore we have to normalize one current, say $I_M = 1$. The same applies to the weighing coefficients, thus we set $c_M = 1$.

We start with the spinning scheme to figure out the restrictions on the currents and the weighing coefficients for zero offset error. First we apply the ideas of Section 5 explicitly to Hall plates with $N = 6$, 8, and 10. We compute the total signal, which is a large sum over all operating phases and contact pairs. The terms in the sum are currents multiplied by weighing factors multiplied by elements of the resistance matrix. We replace

$$R_{i,j} = \begin{cases} R_{i,j}\left(B_{\perp}\right) & \text{if } i \leq j \\ R_{j,i}\left(-B_{\perp}\right) & \text{if } i > j \end{cases} \tag{27}$$
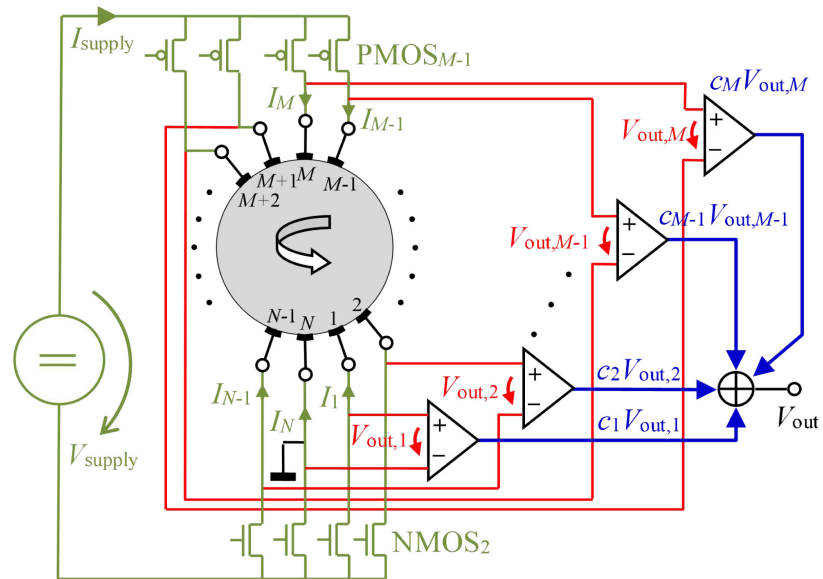
Figure 12. Regular circular Hall plate with $N = 2M$ contacts and circuit for operating mode "multiple input currents, M output voltages". Currents are supplied to the contacts via MOS current sources. Voltages are tapped at M pairs of contacts and summed up with a circuit of M amplifiers. The gains c_k of the amplifiers are weighing coefficients in the linear combination of signals from all output ports.

which is the RMFR principle [20]. At $B_\perp = 0$ the total sum must vanish regardless of the specific numerical values of the resistance matrix. This gives the following necessary conditions

$$I_{N+1-k} = I_k \quad \text{for } k \in [1, M] \tag{28}$$

$$\sum_{k=1}^{M} I_k = 0 \tag{29}$$

(28) means that identical currents have to flow through contacts belonging to the same contact pair. Surprisingly, (28) and (29) are independent of the weighing coefficients. With (28) and (29) the spinning scheme is able to cancel out zero point errors regardless of the symmetry of the Hall plate. Moreover, (28) and (29) and the normalization $I_M = 1$ leave $M - 2$ currents free to choose for maximum SNR. With the $M - 1$ free weighing coefficients we have in total $N - 3$ degrees of freedom (DoF) in the SNR optimization.

From the definition of the SNR in (23) we can start with $SNR = V_{\text{out}}/n_{\text{out}}$. Yet, we need to reconsider the input resistance for a device with many inputs. **Figure 12** shows the circuit where the multi-terminal Hall plate is supplied by multiple current sources. Let us assume as a simplification that an MOS current mirror does not need any drain-source saturation voltage. Then the voltage of the power supply circuit is

$$V_{\text{supply}} = \max_{j=1}^{N} V_j - \min_{j=1}^{N} V_j \tag{30}$$

Note that from all N current sources only two have zero voltage across them—one

at the positive and one at the negative pole of the battery. All others have non-vanishing voltage drop and therefore they all dissipate power. We want to get maximum *SNR* at minimum power dissipation in the *system*, not in the Hall plate alone. Therefore we need to account for the power P_{supply} that is delivered by the power supply circuit.

$$P_{\text{supply}} = V_{\text{supply}} I_{\text{supply}} \tag{31}$$

$$I_{\text{supply}} = \sum_{j=1}^{N} \text{If}\left[I_j > 0; I_j; 0\right] = \frac{1}{2}\left(\left|\sum_{j=1}^{N-1} I_j\right| + \sum_{j=1}^{N-1}\left|I_j\right|\right) \tag{32}$$

This gives us the *SNR* of a multi-port Hall plate with multiple input currents.

$$SNR = \lim_{B_\perp \to 0} \frac{V_{\text{out}}}{n_{\text{out}}} = \mu_H B_\perp \sqrt{\frac{P_{\text{supply}}}{4k_b T \Delta}} \eta_{N-1,M} \tag{33a}$$

$$\eta_{N-1,M} = \frac{\sum_{k=1}^{M}\sum_{j=1}^{M} c_k \left(R_{j,k} - R_{N+1-j,k}\right) I_j}{\sqrt{P_{\text{supply}} R_{\text{out}}} \tan\theta_H} \tag{33b}$$

with the dimension-less noise efficiency $\eta_{N-1,M}$ for the operating mode with $N - 1$ input currents and M output voltages. The output resistance for the circuit in Figure 12 is obtained analogous to Section 3.

$$R_{\text{out}} = \sum_{j=1}^{M} c_j^2 \left(\sum_{k=1}^{M} R_{j,k} - \sum_{k=M+1}^{N-1} R_{j,k} - \sum_{k=1}^{M} R_{N+1-j,k} + \sum_{k=M+1}^{N-1} R_{N+1-j,k}\right) \tag{34}$$

In (33b) and (34) we had to add an *N*-th row to the resistance matrix with $R_{N,k} = 0$ for $k = 1, 2, \cdots, N-1$. Analogous to (4a) we can define an average Hall geometry factor G_H.

$$G_H = \frac{\sum_{k=1}^{M}\sum_{j=1}^{M} c_k \left(R_{j,k} - R_{N+1-j,k}\right) I_j}{M R_{\text{sheet}} \tan\theta_H I_{\text{supply}}} \tag{35}$$

when searching for the optimum currents and weighing coefficients we can reduce their number due to the symmetry of the Hall plates at weak magnetic field. It holds

$$I_{M+1-k} = -I_k \quad \text{and} \quad c_{M+1-k} = c_k \quad \text{for } k \in \left[1, \lfloor M/2 \rfloor\right]. \tag{36}$$

An algorithm is shown in **Appendix F**. The results of this optimization are shown in Figure 13 and Table 3. We note that the maximum achievable *SNR* rises monotonously with the number of contacts. At $N = 40$ and for optimized weighing coefficients it is 89% larger than for conventional Hall plates with four contacts. But even for low *N* the *SNR* improvement is very good: with only eight contacts it is 47%. Another interesting aspect is that it does not bring any benefit if too many contacts are supplied by current: For up to 12 contacts the optimum circuit uses only two identical supply currents connected to contact pairs (1, *M*) and (*M* + 1, *N*). For Hall plates with 14 up to 32 contacts the optimum circuit uses four supply currents connected to contact pairs (1, *M*), (2, *M* − 1), (*M* + 1, *N*), and (*M* + 2, *N* − 1). For more contacts the optimum circuit uses six supply currents. Each pair of further supply contacts has to carry more current. This
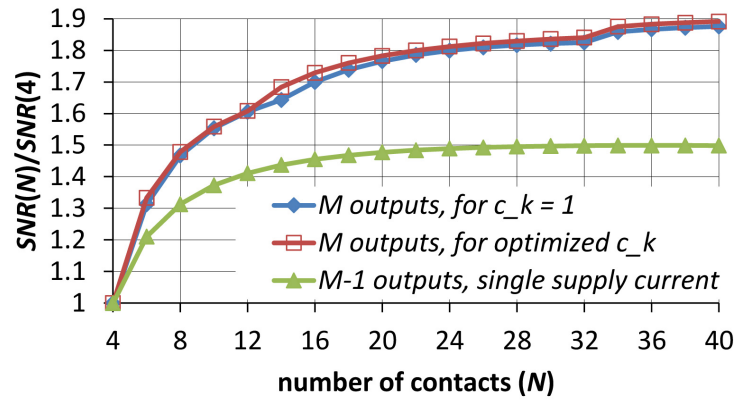
Figure 13. *SNR* versus number of contacts of multi-port Hall plates. Curves labelled "*M* outputs" refer to Hall plates operated in the circuit of **Figure 12**, whereas the curve labelled "*M* − 1 outputs" assumes the circuit from **Figure 6**. The plot shows the ratio of *SNR* for Hall plates with *N* contacts over maximum *SNR* for a Hall plate with four contacts in conventional operating mode of **Figure 1**. Numerical values for "*M* outputs" in **Table 3**. There it is also noted how many supply currents are used and what are the optimum values of these currents. The *SNR* of the curves labelled "*M* outputs" is computed with (33b).

Table 3. Parameters of multi-port Hall plates operated in the circuit of **Figure 12** (computed at 0.09° Hall angle and for $c_k = 1$): number of contacts $N = 2M$, average weak field Hall geometry factor G_{H0}, resistances seen at the supply side and at the output of the circuit (for $R_{\text{sheet}} = 1\ \Omega$), noise efficiency $\eta_{N-1,M}$, and ratio of $SNR(N)$ with N contacts over $SNR(4)$ of conventional Hall plates with only four contacts. We normalized the currents by $I_M = 1$. It holds (28) and (36). Apart from that, all currents which are not explicitly given in the table vanish. Currents are identical for both cases "$c_k = 1$" and "optimum c_k".

N	4	6	8	10	12	14	16	18	20	22
G_{H0}	0.33333	0.49098	0.58403	0.64605	0.69064	0.58209	0.62700	0.66259	0.69156	0.71563
$\dfrac{V_{\text{supply}}}{I_{\text{supply}}}$	0.70763	1.00058	1.19507	1.34224	1.46105	1.00088	1.09431	1.17497	1.24600	1.30955
R_{out}	2.82843	5.66667	9.55583	14.5108	20.5387	27.6433	35.8270	45.0912	55.4370	66.8651
$\eta_{N-1,M}$	0.47123	0.61858	0.69130	0.73193	0.75645	0.77465	0.80109	0.81927	0.83209	0.84125
$\dfrac{SNR(N)}{SNR(4)}$	1	1.31270	1.46701	1.55324	1.60527	1.64388	1.69999	1.73859	1.76578	1.78522
I_{M-1}	−1	0	0	0	0	1.79641	1.76170	1.73860	1.72295	1.71180
N	24	26	28	30	32	34	36	38	40	
G_{H0}	0.73599	0.75345	0.76861	0.78189	0.79365	0.73917	0.75226	0.76404	0.77469	
$\dfrac{V_{\text{supply}}}{I_{\text{supply}}}$	1.36709	1.41971	1.46819	1.51316	1.55510	1.29933	1.33729	1.37302	1.40679	
R_{out}	79.3761	92.9704	107.648	123.410	140.256	158.186	177.201	197.300	218.484	
$\eta_{N-1,M}$	0.84784	0.85257	0.85593	0.85826	0.85982	0.87650	0.87963	0.88200	0.88376	
$\dfrac{SNR(N)}{SNR(4)}$	1.79920	1.80924	1.81637	1.82133	1.82462	1.86002	1.86666	1.87169	1.87543	
I_{M-1}	1.70356	1.69727	1.69237	1.68846	1.68530	1.17899	1.17738	1.17604	1.17490	
I_{M-2}	0	0	0	0	0	2.17131	2.16234	2.15487	2.14858	

leads to potentials at all current input contacts, which are close to V_{supply}, and it leads to potentials at all current output contacts, which are close to ground. Conversely, the benefit of optimized weighing factors is tiny (see **Figure 13**) and not reported in **Table 3**.

7. Experimental Verification

For an experimental verification of our theory, we manufactured the two types of Hall plates in **Figure 14**. A first Hall plate had four contacts and 90° symmetry, a second Hall plate had eight contacts and a 45° symmetry. The active Hall regions were regular octagons with widths of 90.4 μm and 95 μm for first and second Hall plate, respectively. The tubs of the silicon Hall plates had an n-doping profile with a flat peak of $8 \times 10^{15}/cm^3$ (three parts phosphorus and one part arsenic) and a metallurgical thickness of 1.5 μm. The Hall plates were pn-junction isolated with a roughly linear slope of the doping near the junction. At zero reverse bias voltage, the depletion layer reduced the effective thickness of the Hall plates to 0.9 … 1.0 μm. The contacts were made of standard CMOS n-wells and n^+-source/drain diffusions. Opposite contacts of the four-contacts device were spaced apart by 74.6 μm, and their size was 31 μm × 1.3 μm. Opposite contacts of the eight-contacts device were spaced apart by 72 μm and had a size of 11 μm × 9 μm. Unfortunately, we do not know the exact depth profile of the CMOS wells implanted through the small LOCOS openings of the n^+ diffusions. This gives an uncertainty in the contact resistances of the Hall plates, which makes an exact quantitative comparison to our theory impossible. Yet, at least we can give a qualitative comparison in the following.

According to measurements at room temperature, the resistance between opposite contacts of the four-contacts device is 5856 Ohm at small supply voltage. For the eight-contacts device we measured 6930 Ohm at small supply voltage. Both times the resistance increases by 5.5% if the positive supply contact is at 1 V due to the junction field effect at the pn-isolation. For the eight-contacts Hall plate we measured the equivalent resistor network $r_{1,N} = 6562$ Ohm, $r_{2,N} = 46,591$

(a)   **(b)**
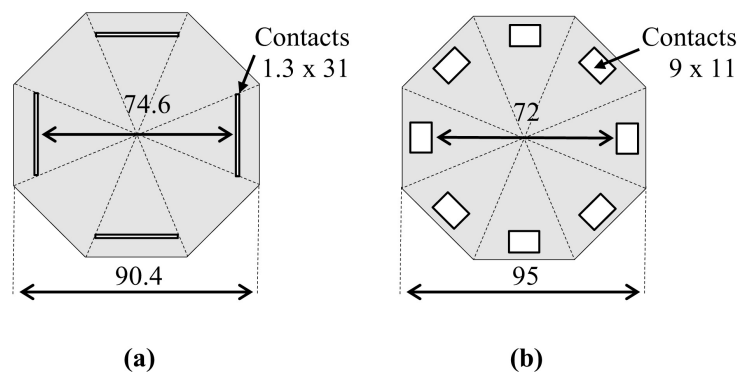
Figure 14. Symmetric octagonal Hall plates with four and eight contacts fabricated in a BiCMOS silicon technology. All lengths in units of μm. They are junction isolated at the perimeter and at the bottom. At the top there is no pn-junction but simply a dielectric insulating layer.

Ohm, $r_{3,N} = 96{,}680$ Ohm, $r_{4,N} = 89{,}165$ Ohm at small supply voltage. Then we reconstructed the network with lumped resistors $r_{1,N} = 6.2$ kOhm, $r_{2,N} = 47$ kOhm, $r_{3,N} = 100$ kOhm, $r_{4,N} = 92$ kOhm. This gave a resistance of 6680 Ohm between opposite contacts. At 1 V supply voltage the Hall output signal of the four-contact device is 58 μV per milli-Tesla of magnetic flux density. The same supply voltage and magnetic flux density give 53.9 μV at ports 1 and 3 and 62.3 μV at port 2 (which is at $cm = 0.5$) of the eight-contacts Hall plate.

We built an electronic circuit according to the operating mode of **Figure 6**. The signals of the three ports are summed up by low-noise integrated electrometer amplifier circuits AD8429 from Analog Devices, Inc. (see **Figure 15**) [22]. The 600 Ohm resistors at the inputs of each AD8429 define the amplification factors $c_1 = c_2 = c_3 = 11$. The inputs of the three AD8429s were connected to the three ports of the eight-contacts Hall plate and the noise in the output of the circuit in **Figure 15** was measured by a 2 MHz DSP lock-in amplifier SR865 from Stanford Research Systems, Inc. [23]. Afterwards, all three inputs of the circuit in **Figure 15** were connected to the single output port of the four-contacts Hall plate, which gives an amplification factor 33. Both times, the Hall plates were supplied by a 1.5 V battery and placed inside a steel box to reduce line interference. We assembled the Hall plates in non-magnetic packages, and we conducted the measurements at ambient temperature. We divided the measured noise voltage spectra by the magnetic sensitivities of the Hall plates and the gain factors of the circuit to get the equivalent magnetic noise. These spectra are plotted in **Figure 16**.

First, we shorted all inputs of the three AD8429s, and measured a white noise voltage spectral density of 33×3 nV/sqrt(Hz) at the output of the circuit in **Figure 15**. Then, we connected three 10 kOhm resistors at the inputs of the three AD8429s, and measured 33×9.2 nV/sqrt(Hz). This is 24% larger than for ideal
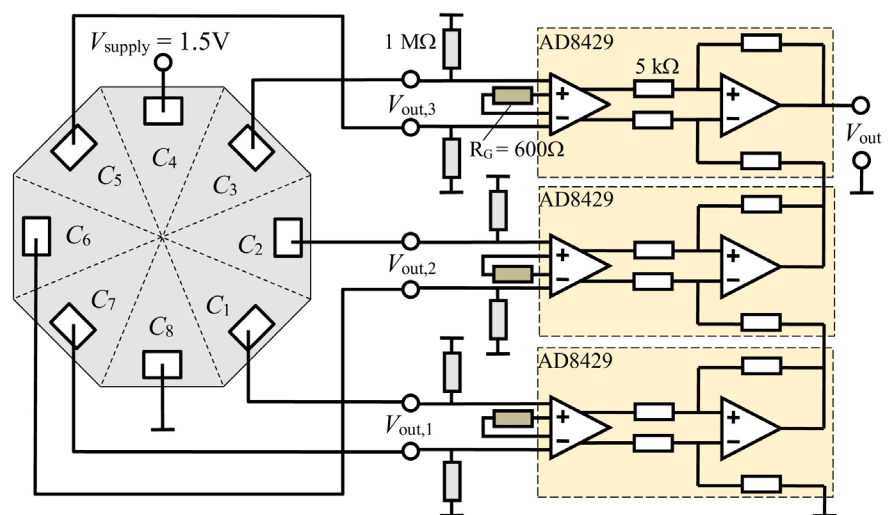
Figure 15. Electronic circuit that amplifies the port voltages of the eight-contacts Hall plate times eleven and sums them up. The operating mode of the Hall plate is the same as in **Figure 6**. Resistors of the same color are equal.
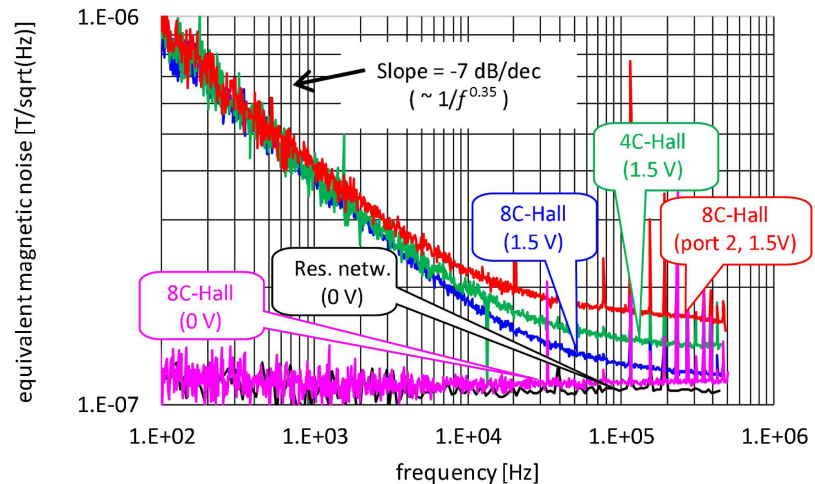
Figure 16. Noise spectral densities measured on the Hall plates from **Figure 14** with the circuit from **Figure 15** at room temperature. The noise voltages were divided by the measured magnetic sensitivities to give the equivalent magnetic noise (for the resistor network the sensitivity of the eight-contacts Hall plate at 1.5 V supply voltage was used). "8C-Hall" denotes the eight-contacts Hall plate, "4C-Hall" the four-contacts Hall plate, and "Res. netw." denotes the equivalent resistor network for the eight-contacts Hall plate. "8C-Hall (port 2)" means that all three AD8429 amplifier inputs were connected to port 2 of the eight-contacts Hall plate. No battery was connected to the Hall plate and to the resistor network for the two flat curves. In all other cases the Hall plates were supplied with 1.5 V battery voltage. At high frequencies the measured noise of the eight-contacts Hall plate is 18.3% lower than of the four-contacts Hall plate in spite of the lower current through the eight-contacts Hall plate.

noiseless amplifiers. Then we connected all inputs of the three AD8429s to a single 10 kOhm resistor, which increased the impedance level times three. In this mode there is the strongest correlation between all three channels. This led to 33 × 19.1 nV/sqrt(Hz) at the output, which is 48% larger than for a noiseless circuit. To sum up, the noise of our circuit is not negligible. However, this is irrelevant if we compare noise measurements of Hall plates with identical impedances. Yet, if a Hall plate has larger output resistance, the noise input current of the circuit will add its own noise.

The measured noise spectra of Hall plates are plotted in **Figure 16**. First, we note that only the spectra of the Hall plates powered up by battery have marked 1/f-noise contributions. The amplifier circuit and the lumped resistors have no 1/f-noise in the relevant region of frequencies. The 1/f-noise corner frequency is near 30 kHz for the eight-contacts Hall plate and lower for the others. Thus, a single operating phase of a spinning scheme should last shorter than 16.7 μs to remove all 1/f-noise.

Second, we note that the noise at 450 kHz of the eight-contacts Hall plate with 1.5 V battery supply is slightly larger than without any battery (10.2 versus 9.8 nV/sqrt(Hz)). This difference of 4.1% can be explained by the 8.2% larger impedance of the Hall plate at 1.5 V supply voltage.

The equivalent resistor network has slightly lower noise: 9.2 nV/sqrt(Hz) at

340 kHz. This is 6.1% less than for the unpowered Hall plate. The resistor network has only 3.6% smaller input resistance than the unpowered Hall plate, which could explain 1.8% smaller noise voltage at port 2. The discrepancy between 1.8% and 6.1% may come from the fact that the lumped resistors deviate up to 6% from the exact values for the equivalent resistor network (see reported values above).

Anyhow, the discrepancy is much smaller than the differences in noise of powered Hall plates. At 1.5 V supply voltage and 450 kHz the equivalent magnetic noise of the circuit with the four-contacts Hall plate was 142 nT/sqrt(Hz), whereas it was only 120 nT/sqrt(Hz) for the circuit with the eight-contacts Hall plate. Thus, the eight-contacts Hall plate has 18.3% better *SNR* despite its lower supply current. Of course, if we use only port 2 of the eight-contact Hall plate, its noise is worse than for the four-contact Hall plate.

The input resistance of the eight-contacts Hall plate is also 18.3% larger than for the four-contacts Hall plate. If we would make the eight-contacts Hall plate thicker by 18.3% it had identical supply current as the four-contacts Hall plate at 1.5 V supply voltage and its SNR would increase by another 8.8%. Then the eight-contacts Hall plate in operating mode according to Figure 6 would have 28.7% better *SNR* at identical power dissipation. This matches closely the predicted 31.3% from Table 2.

Moreover, we measured the residual offset of the eight-contacts Hall plate according to the spinning scheme of Section 5. Thereby we did *not* use the circuit of Figure 15. Instead, we supplied the current with a precision current source and measured voltages at the three ports with a single precision voltmeter. The contacts of the Hall plate were switched by a relais matrix with low thermo-voltages. The Hall plates were assembled in non-magnetic packages, and placed in double shielded zero-Gauss chambers at room temperature. The measured output voltages of the Hall plates were summed up according to (24) and (25). Yet, in (25) the sum extended to $2M$ instead of only M, to cancel out thermo-voltages. The result was divided by the measured magnetic sensitivity to obtain the residual offset equivalent magnetic field. We measured eight devices from a single wafer, and the standard deviation of the results is plotted versus supply voltage in Figure 17. The curve is similar to classic Hall plates with four contacts (as shown in Figure 11 in [6]): the residual offset increases with the supply voltage. The origin seems to be electrical non-linearity and self-heating of the Hall plates, which are not accounted for in our linear theory. Nevertheless, the residual offset is small: at 1 V supply voltage it is 3 µT, at 1.5 V it is 6 µT, and at 2 V it is 10 µT.

To sum up, this experimental section proves that multi-port Hall plates have less thermal noise at identical power dissipation and comparable residual offset to classic Hall plates with four contacts.

8. Discussion

We studied two circuits for multi-port Hall plates. One has a single input current and $M - 1$ output voltages (Figure 6), and the other one has multiple input
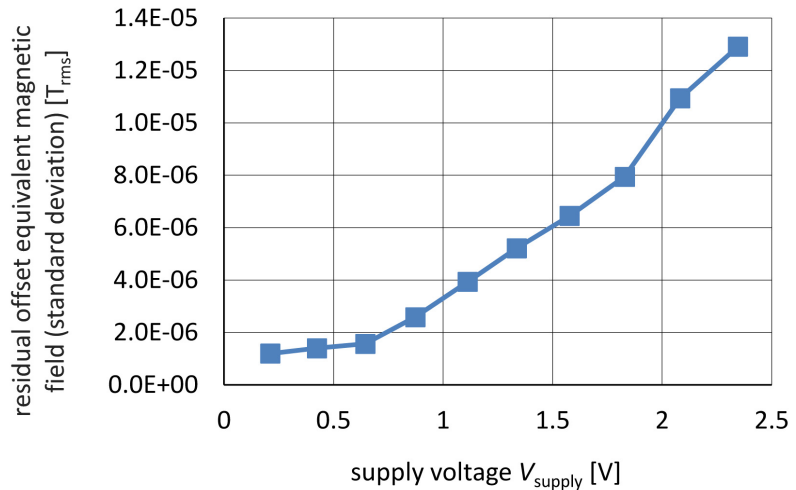
Figure 17. Residual offset equivalent magnetic field of the eight-contacts Hall plate from **Figure 14** measured at room temperature. The spinning scheme of (24), (25) was applied, yet, with M replaced by $2M$ in (25). Note that we use supply voltage on the horizontal axis instead of supply current, because the main origin for residual offset error is the reverse biased pn-isolation junction at the bottom of the Hall plate. Nevertheless, the spinning scheme used constant supply current in all operating phases.

currents and M output voltages (**Figure 12**). The first one shows an improvement in *SNR* of 50% the second one of 90%—both compared to the classical Hall plate with four contacts. Moreover, both circuits are compatible with spinning schemes, which cancel out offset errors as long as the resistances do no depend on the applied voltages. However, the full improvement in *SNR* holds only for large numbers of contacts ($N = 36$). Therefore, the spinning scheme needs to sum up the output signals of many operating phases, which reduces the signal bandwidth. This is the price we have to pay for low noise. However, the second circuit shows remarkable *SNR* improvement of 47% for Hall plates with only eight contacts, two current sources, and four voltmeters (cf. **Table 3**). Moreover, it is possible to move the spinning scheme from the simple classic forward path into a feedback path, where it has only a minor effect on signal bandwidth [24] [25]. For sensor systems with mega-Hertz bandwidth it is best to add pick-up coils for signals beyond 5 kHz and use the Hall plates only for dc to 5 kHz [26]. These systems have unprecedented *SNR*, zero point accuracy, and linearity at low costs [27]—better than modern tunnel-magneto-resistors (TMRs).

We have not touched upon Hall plates with odd numbers of contacts, but their treatment is straightforward and analogous to this paper.

So far, we have applied our theory only to Hall plates with contacts equally large as spacings between them, according to (2). For classical Hall plates with four contacts, this is known to give the best *SNR* per Watt [4]. However, it is not yet clear if this also gives optimum *SNR* per Watt for larger number of contacts.

One can readily apply our theory to *SNR* optimization and spinning schemes of Vertical Hall effect devices [28]. The only difference is that Vertical Hall effect devices have less symmetry in their contact arrangement. This will lead to smaller

SNR at the same power.

In this paper we have not dealt with important practical aspects of the circuits in Figure 6 and Figure 12. Mismatches of current sources can be handled with dynamic element matching, a well-known technique of precision analogue circuit design. The large number of amplifiers does not necessarily imply large chip area, if one uses operational trans-conductance amplifiers, and simply splits the traditional large input stage into *M* smaller input stages. The same applies for the switches of the spinning scheme. This does neither cost additional current nor space, except for some moderate wiring overhead.

9. Conclusion

We have shown by calculation that under a given supply voltage and current drain a regular multi-port Hall plate can achieve up to 90% better signal-to-noise ratio (*SNR*) than classical Hall plates with four contacts. Alternatively, it can provide the same *SNR* at 3.6 times smaller power consumption. An experiment on a non-optimized silicon Hall plate with eight contacts showed 29% better *SNR* than for a classic Hall plate with four contacts, at identical power dissipation. The proposed optimum Hall plates have a regular shape with $2M$ identical contacts. Current flows through one, two, four, or more pairs of contacts, depending on the number of contacts and on which circuit is used (Figure 6 or Figure 12). Voltages are tapped at M (Figure 12) or $M - 1$ (Figure 6) output ports and summed up by a signal conditioning circuit. We also showed spinning schemes, which eliminate zero point errors (offset errors) in Hall plates where the approximations of constant conductivity and thermal equilibrium hold. With an eight-contacts Hall plate, we measured a residual offset error of a few micro-Tesla. The theory was worked out on circular shapes of Hall plates, but other shapes like hexagons, octagons, and regular polygons can be found with conformal transformation. Comparison with various types of Hall plates reported in the literature suggests that the multi-port Hall plate is not just yet another option out of a myriad of existing solutions. Up to day it is the only way to use Hall-effect devices with such a greatly improved noise performance.

Acknowledgements

Conflicts of Interest

The author declares no conflicts of interest regarding the publication of this paper.

References

[1] Burckhardt, C.B. and Strutt, M.J.O. (1964) Noise in Nonreciprocal Two Ports Based

on Hall Effect. *IEEE Transactions on Electron Devices*, **11**, 47-50.
https://doi.org/10.1109/T-ED.1964.15281

[2] Stoessel, Z. and Resch, M. (1993) Flicker Noise and Offset Suppression in Symmetric Hall Plates. *Sensors and Actuators A*: *Physical*, **37-38**, 449-452.
https://doi.org/10.1016/0924-4247(93)80076-S

[3] Mosser, V., Matringe, N. and Haddab, Y. (2017) A Spinning Current Circuit for Hall Measurements down to the Nanotesla Range. *IEEE Transactions on Instrumentation and Measurement*, **66**, 637-650.
https://doi.org/10.1109/TIM.2017.2649858

[4] Ausserlechner, U. (2017) The Signal-to-Noise Ratio and a Hidden Symmetry of Hall Plates. *Solid-State Electronics*, **135**, 14-23. https://doi.org/10.1016/j.sse.2017.06.007

[5] Wick, R.F. (1954) Solution of the Field Problem of the Germanium Gyrator. *Journal of Applied Physics*, **25**, 741-756. https://doi.org/10.1063/1.1721725

[6] Ausserlechner, U. (2016) Hall Effect Devices with Three Terminals: Their Magnetic Sensitivity and Offset Cancellation Scheme. *Journal of Sensors*, Article ID: 5625607.
https://doi.org/10.1155/2016/5625607

[7] Ausserlechner, U. (2018) An Analytical Theory of Hall-Effect Devices with Three Contacts. *Open Physics Journal*, **4**, 14-42.
https://doi.org/10.2174/1874843001804010014

[8] Van Der Meer, J.C., Riedijk, F.R., van Kampen, E., Makinwa, K.A. and Huijsing, J.H. (2005) A Fully Integrated CMOS Hall Sensor with with a 3.65 µT 3 sigma Offset for Compass Applications. 2005 *IEEE International Digest of Technical Papers. Solid-State Circuits Conference*, San Francisco, 10 February 2005, 246-247.

[9] van der Meer, J., Riedijk, F., Makinwa, K. and Huijsing, J. (2007) Standard CMOS Hall-Sensor with Integrated Interface Electronics for a 3D Compass Sensor. *SENSORS*, 2007 *IEEE*, Atlanta, 28-31 October 2007, 1101-1104.
https://doi.org/10.1109/ICSENS.2007.4388598

[10] Munter, P.J.A. (1992) Spinning-Current Method for Offset Reduction in Silicon Hall Plates. Ph.D. Thesis, Delft University of Technology, Netherlands.

[11] Munter, P.J.A. (1990) A Low-Offset Spinning-Current Hall Plate. *Sensors and Actuators A*: *Physical*, **22**, 743-746. https://doi.org/10.1016/0924-4247(89)80069-X

[12] Higgs, J.K. and Humenick, J. (1986) Integrated Circuit with Stress Isolated Hall Element. US Patent No. 4578692.

[13] Kammerer, J.B., Hébrard, L., Frick, V., Poure, P. and Braun, F. (2003) Horizontal Hall Effect Sensor with High Maximum Absolute Sensitivity. *IEEE Sensors Journal*, **3**, 700-707. https://doi.org/10.1109/JSEN.2003.820347

[14] Heidari, H., Gatti, U. and Maloberti, F. (2015) Sensitivity Characteristics of Horizontal and Vertical Hall Sensors in the Voltage-and Current-Mode. 2015 11*th Conference on Ph.D. Research in Microelectronics and Electronics*, Glasgow, 29 June-2 July 2015, 330-333. https://doi.org/10.1109/PRIME.2015.7251402

[15] Homentcovschi, D. and Bercia, R. (2018) Analytical Solution for the Electric Field in Hall Plates. *Zeitschrift für Angewandte Mathematik und Physik*, **69**, Article No. 97. https://doi.org/10.1007/s00033-018-0989-7

[16] Homentcovschi, D. and Murray, B.T. (2019) Explicit Resistance Matrix for a Hall Disk with Multiple Peripheral Contacts: Application to a van der Pauw Type Method For Extended Contacts. *Sensors and Actuators A*: *Physical*, **294**, 1-7.
https://doi.org/10.1016/j.sna.2019.04.027

[17] Ausserlechner, U. (2019) The Classical Hall Effect in Multiply-Connected Plane Re-

gions Part I: Topologies with Stream Function. *Journal of Applied Mathematics and Physics*, **7**, 1968-1996. https://doi.org/10.4236/jamp.2019.79136

[18] Nyquist, H. (1928) Thermal Agitation of Electric Charge in Conductors. *Physical Review*, **32**, 110. https://doi.org/10.1103/PhysRev.32.110

[19] Johnson, J.B. (1928) Thermal Agitation of Electricity in Conductors. *Physical Review*, **32**, 97. https://doi.org/10.1103/PhysRev.32.97

[20] Cornils, M. and Paul, O. (2008) Reverse-Magnetic-Field Reciprocity in Conductive Samples with Extended Contacts. *Journal of Applied Physics*, **104**, Article ID: 024505. https://doi.org/10.1063/1.2951895

[21] Garg, J. and Carlin, H. (1965) Network Theory of Semiconductor Hall-Plate Circuits. *IEEE Transactions on Circuit Theory*, **12**, 59-73. https://doi.org/10.1109/TCT.1965.1082370

[22] https://www.analog.com/media/en/technical-documentation/data-sheets/AD8429.pdf

[23] https://www.manualslib.com/manual/1027268/Stanford-Research-Systems-Sr865.html

[24] Motz, M., Ausserlechner, U., Bresch, M., Fakesch, U., Schaffer, B., Reidl, C., *et al.* (2012) A Miniature Digital Current Sensor with Differential Hall Probes Using Enhanced Chopping Techniques and Mechanical Stress Compensation. *SENSORS*, 2012 *IEEE*, Taipei, 28-31 October 2012, 1-4. https://doi.org/10.1109/ICSENS.2012.6411161

[25] Jiang, J., Kindt, W.J. and Makinwa, K.A. (2014) A Continuous-Time Ripple Reduction Technique for Spinning-Current Hall Sensors. *IEEE Journal of Solid-State Circuits*, **49**, 1525-1534. https://doi.org/10.1109/JSSC.2014.2319252

[26] Ausserlechner, U. (2012) Integrated Circuit Including a Magnetic Field Sensitive Element and a Coil. US Patent No. 8253414.

[27] Jiang, J. and Makinwa, K.A. (2016) Multipath Wide-Bandwidth CMOS Magnetic Sensors. *IEEE Journal of Solid-State Circuits*, **52**, 198-209. https://doi.org/10.1109/JSSC.2016.2619711

[28] Popovic, R.S. (1984) The Vertical Hall-Effect Device. *IEEE Electron Device Letters*, **5**, 357-358. https://doi.org/10.1109/EDL.1984.25945

[29] Carlin, H.J. and Giordano, A.B. (1964) Network Theory: An Introduction To Reciprocal and Non-Reciprocal Circuits. Section 5.1, Prentice Hall, Upper Saddle River, NJ.

[30] Ausserlechner, U. (2019) Relations between Hall Plates with Complementary Contact Geometries. *Journal of Applied Mathematics and Physics*, **7**, 2836-2867. https://doi.org/10.4236/jamp.2019.711195

[31] Ausserlechner, U. (2016) Closed Form Expressions for Sheet Resistance and Mobility from Van-der-Pauw Measurement on 90˚ Symmetric Devices with Four Arbitrary Contacts. *Solid-State Electronics*, **116**, 46-55. https://doi.org/10.1016/j.sse.2015.11.030

Appendix A

Here we compute the resistor network for a multi-port Hall plate of **Figure 6**. First we underline that a Hall plate exposed to magnetic field is non-reciprocal, which means that in general its impedance matrix has no symmetry. Yet, with (20a-c) we can decompose it into the sum of an even- and an odd-symmetric impedance matrix. The even one corresponds to a resistor network and the odd one to a gyrator network. Both networks are connected in series, because the sum of their impedance matrices gives the original one of the Hall plate [29]. Here we discuss only the resistor network, because the gyrator network does not contribute to the noise in the output signal.

Due to the symmetry of our multi-port Hall plates in **Figure 6** the resistor network has only M different values of resistances. From all resistors $r_{i,j}$ between contacts i and j we only need to consider the ones $r_{j,N}$ connected to the N-th contact. All others are again given by the symmetry. For the calculation we assume an operation of the Hall plate according to **Figure A1**, where all contacts 1 to $N-1$ are tied to the same potential V_{supply} and the N-th contact is grounded. Since all contacts 1 to $N-1$ are at identical potential, no current flows between them. Thus, the current into each of these contacts j is proportional to $1/r_{j,N}$. From

$$\begin{pmatrix} I_1 \\ \vdots \\ I_{N-1} \end{pmatrix} = \boldsymbol{g} \cdot \begin{pmatrix} V_{\text{supply}} \\ \vdots \\ V_{\text{supply}} \end{pmatrix} \quad \text{with } \boldsymbol{g} = \left(\boldsymbol{R}_{\text{even}} \right)^{-1} \tag{A1}$$

it follows

$$r_{j,N} = \frac{1}{\sum\limits_{k=1}^{N-1} g_{j,k}} \tag{A2}$$

Table A1 gives numerical values for these resistances at vanishing magnetic
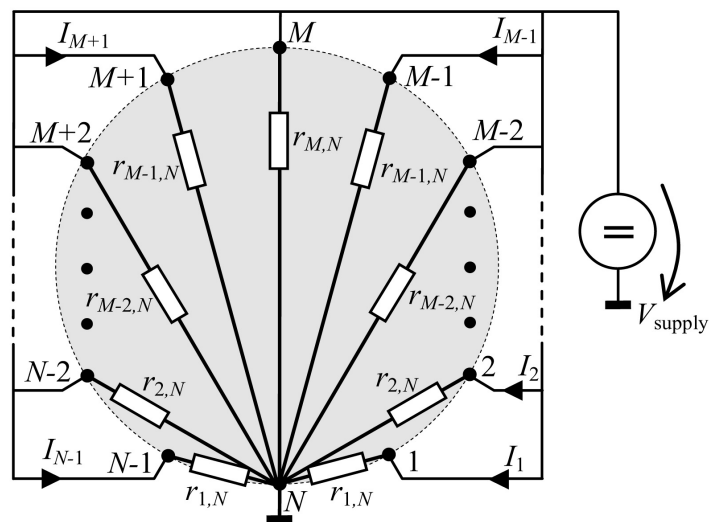
Figure A1. A circuit to compute the resistor network of the Hall plates from **Figure 6**.

Table A1. Resistances $r_{j,N}$ in the resistor networks of Hall plates of **Figure 6** (computed at zero Hall angle and $R_{sheet} = 1\ \Omega$). Each line corresponds to a Hall plate with N contacts. Resistances of contacts with larger index than $N-1$ do not exist—they are labelled as non applicable "n.a.". *Example*: A Hall plate with $N = 8$ contacts has 7 resistors connected to each contact but only the first four have different resistance values. Due to symmetry it holds $r_{5,N} = r_{3,N}$ and $r_{6,N} = r_{2,N}$ and and $r_{7,N} = r_{1,N}$.

N	$r_{1,N}$	$r_{2,N}$	$r_{3,N}$	$r_{4,N}$	$r_{5,N}$	$r_{6,N}$	$r_{7,N}$	$r_{8,N}$	$r_{9,N}$	$r_{10,N}$
3	1.73205	$r_{1,N}$	n.a.	n.a.	n.a.	n.a.	n.a.	n.a.	n.a.	n.a.
4	2.00000	4.82843	$r_{1,N}$	n.a.	n.a.	n.a.	n.a.	n.a.	n.a.	n.a.
5	2.12663	6.88191	$r_{2,N}$	$r_{1,N}$	n.a.	n.a.	n.a.	n.a.	n.a.	n.a.
6	2.19615	8.19615	11.19615	$r_{2,N}$	$r_{1,N}$	n.a.	n.a.	n.a.	n.a.	n.a.
7	2.23833	9.06283	14.53565	$r_{3,N}$	$r_{2,N}$	$r_{1,N}$	n.a.	n.a.	n.a.	n.a.
8	2.26582	9.65685	17.04789	20.10936	$r_{3,N}$	$r_{2,N}$	$r_{1,N}$	n.a.	n.a.	n.a.
9	2.28471	10.07894	18.94221	24.72730	$r_{4,N}$	$r_{3,N}$	$r_{2,N}$	$r_{1,N}$	n.a.	n.a.
10	2.29825	10.38842	20.38842	28.47859	31.56876	$r_{4,N}$	$r_{3,N}$	$r_{2,N}$	$r_{1,N}$	n.a.
11	2.30828	10.62152	21.50956	31.51551	37.46256	$r_{5,N}$	$r_{4,N}$	$r_{3,N}$	$r_{2,N}$	$r_{1,N}$
12	2.31591	10.80119	22.39230	33.98341	42.46870	45.57452	$r_{5,N}$	$r_{4,N}$	$r_{3,N}$	$r_{2,N}$
13	2.32186	10.94246	23.09767	36.00288	46.70167	52.74307	$r_{6,N}$	$r_{5,N}$	$r_{4,N}$	$r_{3,N}$
14	2.32658	11.05544	23.66900	37.66900	50.28257	59.01143	62.12672	$r_{6,N}$	$r_{5,N}$	$r_{4,N}$
15	2.33039	11.14717	24.13755	39.05538	53.32123	64.46840	70.56945	$r_{7,N}$	$r_{6,N}$	$r_{5,N}$
16	2.33351	11.22264	24.52615	40.21872	55.91128	69.21479	78.10392	81.22536	$r_{7,N}$	$r_{6,N}$
17	2.33610	11.28545	24.85174	41.20278	58.13026	73.34803	84.80086	90.94197	$r_{8,N}$	$r_{7,N}$
18	2.33827	11.33827	25.12707	42.04154	60.04154	76.95600	90.74480	99.74480	102.87047	$r_{8,N}$
19	2.34010	11.38311	25.36186	42.76155	61.69666	80.11526	96.02143	107.69147	113.86076	$r_{9,N}$
20	2.34167	11.42148	25.56362	43.38375	63.13752	82.89128	100.71141	114.85355	123.93336	127.06205
21	2.34302	11.45458	25.73821	43.92474	64.39823	85.33951	104.88786	121.30632	133.13604	139.32590

field. A comparison with published results shows perfect agreement: For regular Hall plates with three contacts ($N = 3$) Equation (9) in [7] states $r_{1,3}/R_{sheet} = K\left(\sqrt{2+\sqrt{3}}/2\right)\big/K'\left(\sqrt{2+\sqrt{3}}/2\right) = 1.73205$ (with $K(x)$ being the complete elliptic integral of the first kind and $K'(x)$ being the complementary one). For regular Hall plates with four contacts ($N = 4$) we use Equation (5a), Equation (5b), Equation (14), Equation (15) in [5] to get $r_{1,4}/R_{sheet} = 2$ and $r_{2,4}/R_{sheet} = 2\left(1+\sqrt{2}\right) = 4.82843$.

All our multi-port Hall plates are symmetric, *i.e.* they do not change if we rotate them by integer multiples of $360°/N$. This also affects the symmetry of the $\boldsymbol{g}$ matrix. In **Figure A2** we connect all contacts to ground potential except contact 1, where we apply *negative* supply voltage. It holds

$$\begin{pmatrix} I_N \\ I_1 \\ \vdots \\ I_{N-2} \end{pmatrix} = V_{supply} \begin{pmatrix} -\sum_{j=1}^{N-1} r_{j,N}^{-1} \\ r_{1,N}^{-1} \\ \vdots \\ r_{N-1,N}^{-1} \end{pmatrix} = \boldsymbol{g} \cdot \begin{pmatrix} -V_{supply} \\ 0 \\ \vdots \\ 0 \end{pmatrix} \tag{A3}$$
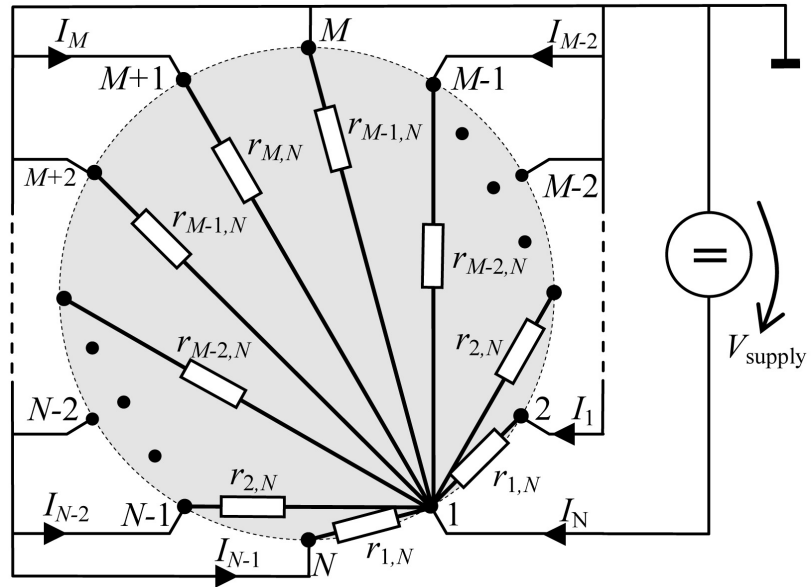
Figure A2. A circuit for studying the symmetry of the g matrix of the symmetrical multi-port Hall plates from **Figure 6**. Due to symmetry all currents are identical to **Figure A1**. The potentials on all contacts are zero except for contact 1, where the potential is $(-1) \times V_{\text{supply}}$.

where the currents $I_1, I_2, \cdots, I_N$ are the currents flowing into contacts $1, 2, \cdots, N$ in **Figure A1**. Comparison of (A1) and (A3) shows that $g_{j,1} = g_{j+1,2}$ for $j > 1$. Continuation of this process means to apply negative supply voltage merely to contact 2, then to contact 3, and so on. Collecting all identities for $g_{i,j}$ gives

$$
g = \left(R_{\text{even}} \right)^{-1} = \begin{pmatrix}
g_{11} & -r_{1,N}^{-1} & -r_{2,N}^{-1} & -r_{3,N}^{-1} & -r_{4,N}^{-1} & \cdots \\
-r_{1,N}^{-1} & g_{11} & -r_{1,N}^{-1} & -r_{2,N}^{-1} & -r_{3,N}^{-1} & \cdots \\
-r_{2,N}^{-1} & -r_{1,N}^{-1} & g_{11} & -r_{1,N}^{-1} & -r_{2,N}^{-1} & \cdots \\
-r_{3,N}^{-1} & -r_{2,N}^{-1} & -r_{1,N}^{-1} & g_{11} & -r_{1,N}^{-1} & \cdots \\
-r_{4,N}^{-1} & -r_{3,N}^{-1} & -r_{2,N}^{-1} & -r_{1,N}^{-1} & g_{11} & \cdots \\
\vdots & \vdots & \vdots & \vdots & \vdots & \ddots
\end{pmatrix}
\tag{A4}
$$

with $g_{11} = \sum_{j=1}^{N-1} r_{j,N}^{-1}$. Thus, g is a Toeplitz matrix with positive elements on the main diagonal and all other elements being negative. This holds also for the definite conductance matrix $G = R^{-1}$ at arbitrary magnetic field. g has even symmetry and $r_{j,N} = r_{N-j,N}$.

Appendix B

Figure 4 shows Hall plates with integer multiples of four contacts. Every fifth contact is connected to the same terminal. In total there are four terminals. The device can be operated like a conventional Hall plate, when current flows between terminals of non-neighboring contacts. The Hall output voltage is tapped across the other two terminals. Current flows in arcs between non-neighboring contacts. Whenever an output contact is left or right of the current flow its potential is lifted or lowered, depending on the impressed magnetic field.

These Hall plates can be readily treated with the theory of [16]. For symmetrical circular plates where contacts cover 50% of the perimeter we get from (7)-(10) in the weak field approximation

$$R_{in} = R_{out} = \frac{V_{supply}}{I_{supply}} = \frac{4\sqrt{2}}{N} R_{sheet} \tag{B1}$$

$$G_{H0} = \frac{\sqrt{2}}{3} \frac{R_{in}}{R_{sheet}} = \frac{8}{3N} \tag{B2}$$

Inserting (B2) into (1) gives the Hall output voltage. (B1) and (B2) also mean that the noise efficiency η is equal to the maximum one of Hall plates with four contacts.

$$\eta = \frac{G_{H0}}{\sqrt{R_{in}/R_{sheet}} \sqrt{R_{out}/R_{sheet}}} = \frac{\sqrt{2}}{3} \cong 0.471 \tag{B3}$$

Appendix C

Hall plates from **Figure 5** can be mapped with conformal transformations to Hall plates from **Figure C1(a)**. The idea behind this mapping is to get a Hall plate with homogeneous current density at zero impressed magnetic field. This is achieved by shifting contacts 1 to $M-1$ down and contacts $M+1$ to $N-1$ up, both proportionally to the potential at these contacts. Moreover, the output contacts M and N are folded and their lengths are adjusted so that the same current passes through them as in the original **Figure 5**. Due to the folding, the output contacts do not disturb the homogeneous current density in the Hall region. At small magnetic field all current streamlines are vertical and the potential along horizontal lines is constant. The longest current streamline has length L, and the width of the Hall plate is W.

In **Figure C1(a)** the MOS transistors act as current sources. The potential at one of the contacts $M+1$ to $N-1$ is maximal. If we neglect the saturation voltage of the PMOS transistors when their channels are pinched off, this maximum potential is also at the power supply. All other PMOS transistors on the k-th contact have non-vanishing drain-source voltages equal to $\max(V_j) - V_k$, and therefore they dissipate the power $(\max(V_j) - V_k) * I_k$ for j and k from $M+1$ to $N-1$. The same applies to the NMOS transistors at the negative terminal of the power supply. The NMOS transistor on the k-th contact dissipates the power $(V_k - \min(V_j)) * I_k$ for j and k from 1 to $M-1$. In other words, the power which we save in the Hall plate (a) is dissipated in the current sources! Thus, the system works suboptimally.

In **Figure C1(b)** we replace the Hall plate of **Figure C1(a)** by a circumscribed rectangle of length L and width W. All current contacts at positive supply are fused to a single large contact 3, and all current contacts at the negative supply are fused to a single large contact 1. The output contacts do not change. Due to the new shape we have shifted the power dissipation of the MOS transistors from (a) into the Hall plate (b). The entire circuit uses the same power, but only
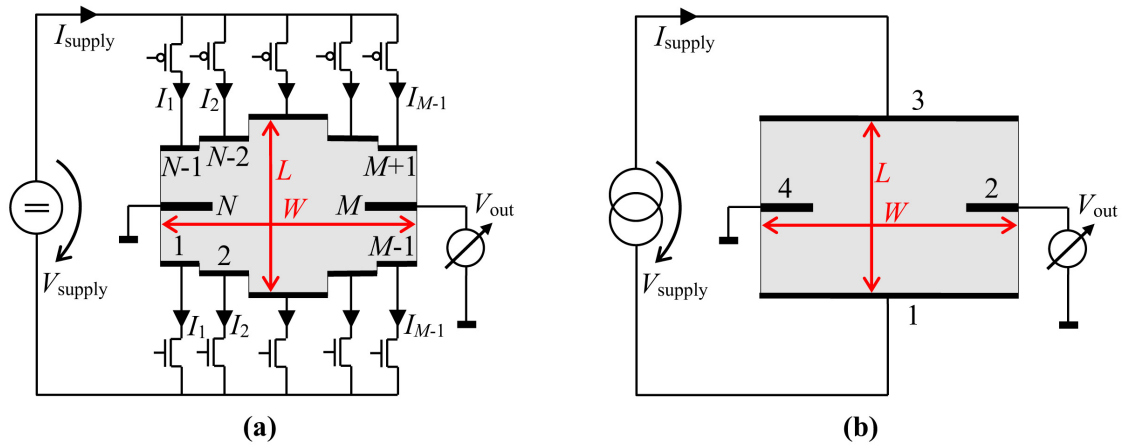
Figure C1. (a) Conformal transformation of the Hall plate from **Figure 5** onto a shape with homogeneous current density at low magnetic field. Current streamlines are straight and vertical, and iso-potential lines are straight and horizontal. The output contacts M and N are folded inside the Hall region. They do not disturb the homogeneous current density. Neglecting the saturation voltage of the MOS current sources the power dissipated by the circuit is $(L/W)R_{\text{sheet}}I_{\text{supply}}^2$. (b) Classical Hall plate with four contacts having identical input and output resistances as (a) but larger Hall signal and therefore larger *SNR*.

in (b) the total power is available inside the Hall plate. Obviously, in **Figure C1(b)** big portions of contacts 1 and 3 are more distal to the output contacts than in **Figure C1(a)**. Therefore, their short circuiting action on the Hall signal is lower, and this gives larger Hall signal per Hall input current. It means that the Hall plate from [13] has less Hall signal per Watt than a classical Hall plate with four contacts, for which we know the maximum noise efficiency to be $\sqrt{2}/3 \cong 0.471$ [4].

Appendix D

Here we discuss the current mode operation of Hall plates from [14]. **Figure D1(a)** shows their configuration, which consists of two conventional Hall plates with four contacts and 90° symmetry connected in a specific way. Both Hall plates are supplied by a floating current source and their outputs are connected via ampere-meters I_a, I_b to reference potential. The output signal I_{out} is the difference of the readings of both ampere-meters. Since the output contacts are tied to the very same reference potential via the low ohmic ampere-meters, we can skip half of the arrangement—this will double the output resistance and it halves the output signal and the supply voltage at identical supply current (see **Figure D1(b)**). The conductance matrix $G = R^{-1}$ is given in (47) in [30]. Due to the symmetry of the Hall plate it is a Toeplitz matrix with only three different values G_{11}, G_{12}, and G_{21}. It holds

$$\begin{pmatrix} I_1 \\ I_2 \\ I_3 \end{pmatrix} = \begin{pmatrix} G_{11} & G_{12} & -G_{11}-G_{12}-G_{21} \\ G_{21} & G_{11} & G_{12} \\ -G_{11}-G_{12}-G_{21} & G_{21} & G_{11} \end{pmatrix} \cdot \begin{pmatrix} 0 \\ V_{\text{supply}}/2 \\ V_{\text{supply}}/2 \end{pmatrix} \quad \text{(D1)}$$

with $I_{\text{supply}} = I_2 + I_3$ and $I_{\text{out}} = -I_1 - (I_1 + I_2 + I_3)$ it follows for **Figure D1(b)**
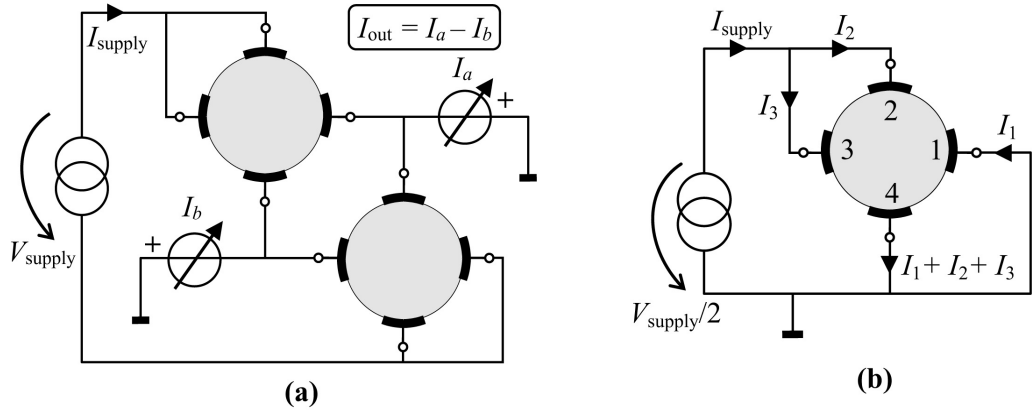
Figure D1. (a) Two Hall plates with four contacts and 90° symmetry are connected for current mode operation in [14]. Due to Kirchhoff's nodal current law $I_a = -I_b$ and therefore $I_{out} = 2I_a$. (b) A single Hall plate with four contacts and 90° symmetry operated in current mode.

$$\frac{I_{out}}{I_{supply}} = \frac{-G_{12} + G_{21}}{2G_{11} + G_{12} + G_{21}} \tag{D2}$$

If we repeat the same procedure for a conventional Hall plate operated the usual way (see **Figure 1**, but contacts are not necessarily 45° large) it holds

$$\begin{pmatrix} 0 \\ I_{supply} \\ 0 \end{pmatrix} = \begin{pmatrix} G_{11} & G_{12} & -G_{11} - G_{12} - G_{21} \\ G_{21} & G_{11} & G_{12} \\ -G_{11} - G_{12} - G_{21} & G_{21} & G_{11} \end{pmatrix} \cdot \begin{pmatrix} V_1 \\ V_{supply} \\ V_3 \end{pmatrix} \tag{D3}$$

with $V_{out} = V_1 - V_3$ it follows for **Figure 1**

$$\frac{V_{out}}{V_{supply}} = \frac{-G_{12} + G_{21}}{2G_{11} + G_{12} + G_{21}} \tag{D4}$$

The R.H.S.s of (D2) and (D4) are identical. Hence, the output signals given in per cent of supply quantities are identical for the current mode operation in **Figure D1(b)** and for the conventional Hall operation in **Figure 1**. Of course the output signal doubles in **Figure D1(a)**, because we send the same current through a second device and add their outputs. The supply voltage and the total power also double. Comparison of (D4) with (1) gives for weak magnetic field

$$\frac{V_{out}}{V_{supply}} = \frac{I_{out}}{I_{supply}} = \frac{G_{H0}}{(L/W)_{eff}} \mu_H B_\perp \tag{D5}$$

where we used the effective number of squares $(L/W)_{eff}$ for the ratio of resistance between two opposite contacts over sheet resistance. G_{H0} is missing in (3) in [14]. In [4] it is shown that Hall plates with four contacts have a maximum possible value for the noise efficiency $G_{H0}/(L/W)_{eff}$, which is $\sqrt{2}/3 \cong 0.471$. In silicon a phosphor doping of $2 \times 10^{16}/cm^3$ gives a Hall mobility of 0.108/T. Therefore conventional silicon Hall plates with 90° symmetry have maximum magnetic field sensitivities of roughly 50 mV/V/T = 5%/T for both kinds of operation, voltage mode and current mode. Again, for **Figure D1(a)** this means 10%/T for the total

circuit with two Hall plates. We have checked this also by 2D-FEM-simulations with COMSOL Multiphysics.

And how about *SNR*? At weak magnetic field the input resistance of a single device in current mode in **Figure D1(b)** is exactly half of the input resistance of the same device operated according to **Figure 1**. This holds for contacts of arbitrary size. We can prove it with the resistor network in [31]: it has resistors $r_{1,4} = R_H$ between all neighboring contacts and resistors $r_{2,4} = 2R_D$ between non-neighboring contacts. Thus, for the same Hall plates the circuits in **Figure D1(a)** and in **Figure 1** consume the same power at identical supply voltage V_{supply}. In **Figure D1(a)** the Hall output current I_{out} and the thermal noise output current $I_{out,noise}$ are given by

$$I_{out} = I_a - I_b = 2 \frac{G_{H0}}{(L/W)_{eff}} \mu_H B_\perp V_{supply} \frac{2R_D + R_H}{2R_D R_H} \tag{D6}$$

$$I_{out,noise} = 2 \sqrt{4k_b T \Delta \frac{6R_D + R_H}{2R_D R_H}} \tag{D7}$$

The noise current flows with opposite polarity through both ampere-meters, and this gives the factor 2 in (D7). The effective output resistance of the circuit in **Figure D1(a)** is $2R_D R_H / (6R_D + R_H)$ and it causes the thermal output noise current according to [18]. The ratio of (D6) over (D7) gives the $SNR^{(current\ mode)}$ of the circuit in **Figure D1(a)**. The $SNR^{(conventional)}$ of a conventional Hall plate with four contacts is given by (23). The ratio of both is

$$\frac{SNR^{(current\ mode)}}{SNR^{(conventional)}} = \sqrt{\frac{2R_D + R_H}{6R_D + R_H}} < 1 \tag{D8}$$

which shows that at the same power consumption the *SNR* of the circuit in **Figure D1(a)** operated in current mode is smaller than the *SNR* of the same Hall plate operated in a conventional way like in **Figure 1**. The conventional Hall plate circuit has maximum *SNR* for $R_H = r_{1,4} = 2R_{sheet}$ and $2R_D = r_{2,4} = 2(1+\sqrt{2})R_{sheet} \cong 4.828R_{sheet}$ (see **Table A1** for $N = 4$). Inserting these values into (D8) shows that the maximum achievable *SNR* of current mode operation is roughly 1.55 times smaller. This finding is consistent with [6], where the maximum achievable *SNR* of symmetric Hall plates with three contacts was found to be 1.51 times lower than of conventional Hall plates with four contacts. After all the current mode operation in **Figure D1** shorts two of the four contacts, thereby making a structure, which effectively has only three terminals. A four-contacts Hall plate with two contacts shorted is similar, but not identical, to a three-contacts Hall plate. This explains the reduction by 1.55 instead of only by 1.51.

Figure D2 shows some other versions of current mode operation. For micro-electronic circuits it is difficult to make perfect shorts, whereas it is simpler to make perfect opens. Therefore, one prefers to measure open loop voltages instead of short circuit currents at the outputs of Hall plates.
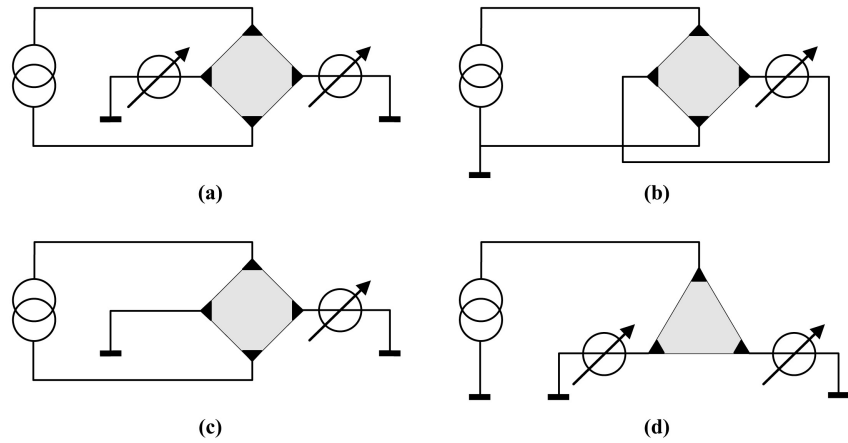
Figure D2. (a-d) Several versions for current mode operation of Hall plates (w/o floating current source, w/o floating ampere-meters). (a) has twice the Hall signal but also twice the noise current than (b) and (c), which gives identical *SNR*. Due to Kirchhoff's nodal current law the currents through both ampere-meters in (a) must have equal magnitude and opposite sign. (d) is the current mode version of **Figure 2**. Both have identical *SNR*.

Appendix E

In Sections 2-5 all amplifiers in **Figure 6** had the same gain. Can we increase the *SNR* further if we look for appropriate values c_k by which we multiply the output signals of the ports prior to summing them up? With (4a) we get the total output voltage

$$V_{\text{out}} = \sum_{k=1}^{M-1} c_k V_{\text{out},k} = R_{\text{sheet}} \tan(\theta_H) I_{\text{supply}} \sum_{k=1}^{M-1} c_k G_{H,k} . \tag{E1}$$

The output resistance also changes. We can recur to **Figure 9**, however, now the ideal transformers have turns ratios $1:c_k$ instead of the original 1:1. If output current I_{out} is injected into the secondary side of the transformers, it gives $c_k \times I_{\text{out}}$ flowing out of the primary sides. Multiplication of these currents with the resistance matrix gives the port voltages. They are present at the primary sides of the transformers, and they will be amplified again by the factor c_k to the secondary side. Thus, the output resistance of port k will appear c_k^2 larger in the total output of the circuit, whereas the Hall signal is amplified only by c_k.

$$R_{\text{out}} = \frac{V_{\text{out}}}{I_{\text{out}}} = \sum_{k=1}^{M-1} c_k^2 \left(\sum_{j=1}^{M-1} R_{k,j} + \sum_{j=M+1}^{N-1} R_{N-k,j} - \sum_{j=1}^{M-1} R_{N-k,j} - \sum_{j=M+1}^{N-1} R_{k,j} \right) \tag{E2}$$

with (23) the *SNR* is proportional to

$$\frac{\displaystyle\sum_{k=1}^{M-1} c_k G_{H,k}}{\sqrt{\displaystyle\sum_{k=1}^{M-1} c_k^2 \left(\sum_{j=1}^{M-1} R_{k,j} + \sum_{j=M+1}^{N-1} R_{N-k,j} - \sum_{j=1}^{M-1} R_{N-k,j} - \sum_{j=M+1}^{N-1} R_{k,j} \right)}} , \tag{E3}$$

where we skipped all terms which are independent of the weighing factors c_k. We look for specific values of all c_k which maximize (E3). First we note from (E3) that once we have an optimum solution for all c_k we can multiply them with a

constant factor without changing (E3). This means that for a unique solution we need to set $c_1 = 1$. We determine the other $M - 2$ weighing factors by taking the square of (E3), differentiating it with respect to c_ℓ, and setting the result equal to zero. This gives a system of $M - 2$ second order algebraic equations for c_ℓ ($2 \leq \ell \leq M - 1$).

$$
G_{H,\ell} \sum_{k=1}^{M-1} c_k^2 \left(\sum_{j=1}^{M-1} R_{k,j} + \sum_{j=M+1}^{N-1} R_{N-k,j} - \sum_{j=1}^{M-1} R_{N-k,j} - \sum_{j=M+1}^{N-1} R_{k,j} \right)
$$
$$
= c_\ell \left(\sum_{j=1}^{M-1} R_{\ell,j} + \sum_{j=M+1}^{N-1} R_{N-\ell,j} - \sum_{j=1}^{M-1} R_{N-\ell,j} - \sum_{j=M+1}^{N-1} R_{\ell,j} \right) \sum_{k=1}^{M-1} c_k G_{H,k}
$$
(E4)

The numerical solution is straightforward (e.g. with Mathematica), if we use different starting values smaller than 1 for all c_k. **Table E1** gives the optimum weighing factors and the relative increase in *SNR* for weighted over non-weighted output signals. Surprisingly, the improvement in *SNR* is only tiny, although the weighing factors deviate notably from 1. We found that the values reported in **Table E1** are independent on the magnitude of the magnetic field. For practical use it seems needless to implement weighing coefficients, because the *SNR* improvement is too small.

Table E1. Noise efficiency $\eta_{1,M-1}$ of Hall plates operated with the circuit of **Figure 6** with optimum weighing coefficients. "ratio" is the *SNR* with optimum c_k over *SNR* with $c_k = 1$. We normalized $c_1 = 1$. For c_k-coefficients the symmetry of (36) holds. All other non-vanishing coefficients are given.

N	8	10	12	14	16	18	20	26	32	40
$\eta_{1,M-1}$	0.62012	0.65014	0.67025	0.68463	0.69539	0.70372	0.71035	0.72388	0.73203	0.73873
ratio	1.00179	1.00441	1.00743	1.01059	1.01378	1.01693	1.02001	1.02867	1.03646	1.04561
c_2	0.88232	0.82854	0.79709	0.77611	0.76094	0.74935	0.74013	0.72085	0.70843	0.69715
c_3	c_1	c_2	0.75000	0.70411	0.67360	0.65161	0.63487	0.60176	0.58162	0.56405
c_4	n.a.	c_1	c_2	c_3	0.64982	0.61377	0.58783	0.53988	0.51262	0.48983
c_5	n.a.	n.a.	c_1	c_2	c_3	c_4	0.57406	0.50681	0.47157	0.44353
c_6	n.a.	n.a.	n.a.	c_1	c_2	c_3	c_4	0.49214	0.44701	0.41309
c_7	n.a.	n.a.	n.a.	n.a.	c_1	c_2	c_3	c_6	0.43378	0.39284
c_8	n.a.	n.a.	n.a.	n.a.	n.a.	c_1	c_2	c_5	0.42960	0.37987
c_9	n.a.	n.a.	n.a.	n.a.	n.a.	n.a.	c_1	c_4	c_7	0.37261
c_{10}	n.a.	n.a.	n.a.	n.a.	n.a.	n.a.	n.a.	c_3	c_6	0.37027

Appendix F

Figure F1 shows a Mathematica script to search for the optimum supply currents and weighing coefficients for Hall plates with $N = 18$ contacts operated in mode "multiple input currents—multiple output voltages". The symmetry of the supply currents is needed for the spinning scheme. The symmetry of the weighing coefficients is a consequence. The results show that currents into contacts 3,

4, 5, 6, 7, 12, 13, 14, 15, 16 vanish. All currents are independent of the weighing coefficients. The noise efficiencies are 0.819275 and 0.829779, respectively.

```
In[109]:= (* Algorithm to optimize supply currents for maximum SNR *)
          (* pre-requisite: the Rmatrix of rank n-1 is given and it was computed for a Hall angle of Pi/2000 *)

          n = 2 * 9 (* set the number of contacts n *)
          Do[c[i] = 1, {i, n / 2}] (* set all weighing coefficients to 1 *)
          Isupply[n / 2] = 1; (* normalize M-th supply current to 1 *)
          Isupply[Ceiling[(n / 2 + 1) / 2]] = 0;
          Do[Isupply[n / 2 + 1 - k] = -Isupply[k], {k, 2, IntegerPart[n / 4]}]
          Isupply[1] = Simplify[-Sum[Isupply[k], {k, 2, n / 2}]]; (* necessary condition for spinning scheme *)
          Table[Isupply[Min[k, n + 1 - k]], {k, 1, n - 1}] (* output all supply currents to check symmetry *)
          (* search for maximum of SNR: *)
          erg1 =
           FindMaximum[
            {Sum[c[k] * (Sum[Rmatrix[[k, j]] * Isupply[Min[j, n + 1 - j]], {j, 1, n - 1}] -
                  If[k > 1, Sum[Rmatrix[[n + 1 - k, j]] * Isupply[Min[j, n + 1 - j]], {j, 1, n - 1}], 0]), {k, 1, n / 2}] /
               Tan[Pi / 2000] /
             Sqrt[1 / 2 * (Sum[Abs[Isupply[Min[j, n + 1 - j]]], {j, 1, n - 1}] + Abs[Sum[Isupply[Min[j, n + 1 - j]], {j, 1, n - 1}]]) *
                (Max[Table[If[k < n, Sum[Rmatrix[[k, j]] * Isupply[Min[j, n + 1 - j]], {j, 1, n - 1}], 0], {k, n}]] -
                 Min[Table[If[k < n, Sum[Rmatrix[[k, j]] * Isupply[Min[j, n + 1 - j]], {j, 1, n - 1}], 0], {k, n}]]) *
                Sum[c[j]^2 * (Sum[Rmatrix[[j, k]], {k, 1, n / 2}] - Sum[Rmatrix[[j, k]], {k, n / 2 + 1, n - 1}] -
                     If[j > 1, Sum[Rmatrix[[n + 1 - j, k]], {k, 1, n / 2}] - Sum[Rmatrix[[n + 1 - j, k]], {k, n / 2 + 1, n - 1}], 0]),
                  {j, 1, n / 2}]]},
             Transpose[{Table[Isupply[k], {k, 2, IntegerPart[n / 4]}], Table[0, {k, 2, IntegerPart[n / 4]}]}],
             Method → "PrincipalAxis"]

          Print["Now with weighing coefficients: "]
          Clear[c]
          c[1] = 1; (* normalizes first weighing coefficient *)
          c[n / 2] = 1; (* set M-th coefficient equal to first one for symmetry reasons *)
          Do[c[n / 2 + 1 - k] = c[k], {k, 2, IntegerPart[n / 4]}] (* set symmetry for coefficients *)
          Table[c[k], {k, 1, n / 2}] (* output all M coefficients to check *)
          (* search for new maximum of SNR: *)
          erg2 =
           FindMaximum[
            {Sum[c[k] * (Sum[Rmatrix[[k, j]] * Isupply[Min[j, n + 1 - j]], {j, 1, n - 1}] -
                  If[k > 1, Sum[Rmatrix[[n + 1 - k, j]] * Isupply[Min[j, n + 1 - j]], {j, 1, n - 1}], 0]), {k, 1, n / 2}] /
               Tan[Pi / 2000] /
             Sqrt[1 / 2 * (Sum[Abs[Isupply[Min[j, n + 1 - j]]], {j, 1, n - 1}] + Abs[Sum[Isupply[Min[j, n + 1 - j]], {j, 1, n - 1}]]) *
                (Max[Table[If[k < n, Sum[Rmatrix[[k, j]] * Isupply[Min[j, n + 1 - j]], {j, 1, n - 1}], 0], {k, n}]] -
                 Min[Table[If[k < n, Sum[Rmatrix[[k, j]] * Isupply[Min[j, n + 1 - j]], {j, 1, n - 1}], 0], {k, n}]]) *
                Sum[c[j]^2 * (Sum[Rmatrix[[j, k]], {k, 1, n / 2}] - Sum[Rmatrix[[j, k]], {k, n / 2 + 1, n - 1}] -
                     If[j > 1, Sum[Rmatrix[[n + 1 - j, k]], {k, 1, n / 2}] - Sum[Rmatrix[[n + 1 - j, k]], {k, n / 2 + 1, n - 1}], 0]),
                  {j, 1, n / 2}]]},
             Transpose[{Flatten[{Table[Isupply[k], {k, 2, IntegerPart[n / 4]}], Table[c[k], {k, 2, Ceiling[n / 4]}]}],
               Flatten[{Table[Isupply[k] /. erg1[[2]], {k, 2, IntegerPart[n / 4]}], Table[1, {k, 2, Ceiling[n / 4]}]}]}],
             Method → "PrincipalAxis"]

Out[109]= 18

Out[113]= {-1, Isupply[2], Isupply[3], Isupply[4], 0, -Isupply[4], -Isupply[3], -Isupply[2],
          1, 1, -Isupply[2], -Isupply[3], -Isupply[4], 0, Isupply[4], Isupply[3], Isupply[2]}

Out[114]= {0.819275, {Isupply[2] → -1.7386, Isupply[3] → 0., Isupply[4] → 0.}}

          Now with weighing coefficients:

Out[118]= {1, c[2], c[3], c[4], c[5], c[4], c[3], c[2], 1}

Out[119]= {0.829779, {Isupply[2] → -1.7386, Isupply[3] → 0.,
              Isupply[4] → 0., c[2] → 1.78108, c[3] → 2.03522, c[4] → 1.89789, c[5] → 1.85215}}
```

Figure F1. Mathematica script to search for the optimum supply currents and weighing coefficients for a Hall plates with $N = 18$ contacts operated in mode "multiple input currents—multiple output voltages".